


June 2019

Design and Testing of a Reciprocating Wind Harvester

Ahmet Topcuoglu

University of South Florida, topcu.ahmet01@gmail.com

Follow this and additional works at: <https://scholarcommons.usf.edu/etd>

 Part of the [Oil, Gas, and Energy Commons](#)

Scholar Commons Citation

Topcuoglu, Ahmet, "Design and Testing of a Reciprocating Wind Harvester" (2019). *Graduate Theses and Dissertations*.

<https://scholarcommons.usf.edu/etd/7971>

This Thesis is brought to you for free and open access by the Graduate School at Scholar Commons. It has been accepted for inclusion in Graduate Theses and Dissertations by an authorized administrator of Scholar Commons. For more information, please contact scholarcommons@usf.edu.

Design and Testing of a Reciprocating Wind Harvester

by

Ahmet Topcuoglu

A thesis submitted in partial fulfillment
of the requirements for the degree of
Master of Science in Mechanical Engineering
Department of Mechanical Engineering
College of Engineering
University of South Florida

Major Professor: David W. Murphy, Ph.D.
Rasim Guldiken, Ph.D.
Andres E. Tejada-Martinez, Ph.D.

Date of Approval:
June 20, 2019

Keywords: renewable energy, wind harvesting, flag with frame, regular flapping,
omnidirectional

Copyright © 2019, Ahmet Topcuoglu

DEDICATION

I dedicate my thesis to my beloved wife, Hale Topcuoglu, and my beloved son, Huseyin Topcuoglu. I want to thank to them because of their unbelievable supports being with me in the far away from our home country, Turkey.

I also would like to dedicate my thesis to my father, M. Yasar Topcuoglu who helps me any time with his knowledge, experience, recommendations and supports like my mother and grandmother who send their good wishes every day and taught me to be honest and hardworking as well as being positive, and my brother that has been always with my side with his cheerfulness.

Finally, I would like to dedicate my thesis to my country and my people. I would not have come to the USA for my master's degree if the Republic of Turkey- Ministry of Education had not sponsored me.

To all whom martyrs for the homeland of the Republic of Turkey.

ACKNOWLEDGMENTS

I would like to express the deepest appreciation to my advisor, Dr. David W. Murphy, for his guidance, ideas and continuous supports. It was an honor to work with him who attributes to his students with respectfulness, enthusiasm and endless care. I would also like to thank Dr. Rasim Guldiken for his patience and supports throughout my master program as well as his valuable input in my committee like the third committee member, Dr. Andres E. Tejada-Martinez. I really want to thank my colleagues Ali al Dasouqi for his help in the setup of the high-speed camera and tools with their process, and Ferhat Karakas who encouraged me to study with Dr. Murphy and his endless support for analysis of the images. Finally, I would like to thank to the Department of Mechanical Engineering for the opportunity to use the wind tunnel located in one of the department's lab.

TABLE OF CONTENTS

List of Tables	ii
List of Figures	iii
Abstract	v
Chapter 1: Literature Review	1
1.1 Renewable Energy Harvesting	1
1.2 Wind Energy Harvesting	3
1.2.1 Macro Scale Wind Energy Harvesting (Wind Turbines)	4
1.2.2 Micro Scale Wind Energy Harvesting	6
1.3 Micro Wind Harvester Designs	9
Chapter 2: Model and Design	18
2.1 Introduction	18
2.2 Harvester Concept and Design	18
2.2.1 Concept	19
2.2.2 Design	20
2.2.3 Wind Tunnel and Orientation	21
2.2.4 Methods	22
2.3 Processing and Analysis	24
Chapter 3: Results	26
3.1 Description of Modes	26
3.1.1 Stable	27
3.1.2 Irregular Flapping	28
3.1.3 Regular Flapping	29
3.1.4 Sinuous Motion	30
3.2 Analysis of The Behavior of The Flag in AR, PR, and Re	31
3.3 Analysis of Regular Flapping	33
Chapter 4: Discussion	39
4.1 Comparison of Other Micro Wind Harvesters	39
4.2 Future Design Implementation	40
References	42
Appendix A: Copyright Permissions	45

LIST OF TABLES

Table 1.1 Types of Renewable Energy Harvesting Categorization	1
Table 1.2 Power Density Comparison for Ambient Energy Sources	4
Table 2.1 Experimental Sample Matrix Table	20
Table 3.1 Distribution of Harvester Behaviors in Terms of Parametric Ratio, Aspect Ratio, and Wind Speeds	26
Table 3.2 Experimental Analyzed Values of Flapping Frequency, Flapping Angle, and the Amplitude on the Regular Flapping Samples.....	33

LIST OF FIGURES

Figure 1.1 Hierarchy of Main Energy Harvesting Technologies.....	2
Figure 1.2 Wind Turbine Basic Operation Principle	4
Figure 1.3 A Horizontal-Axis Wind Turbine System Components.....	5
Figure 1.4 Darrieus-Type Wind Turbine	6
Figure 1.5 Common Aeroelastic Mechanisms for Energy Harvesting; (A) Vortex Shedding, (B) Flutter, (C) Galloping, and (D) Flapping Leaf.....	8
Figure 1.6 Configuration of Piezoelectric Windmill Design by Priya.....	10
Figure 1.7 Configuration of a Piezoelectric Compact Wind Turbine.....	11
Figure 1.8 Design of Piezoelectric Wind Harvester with Scotch Yoke Mechanism	11
Figure 1.9 Diagram of Three Different Modes Used in the Design of Dong Jun Li et al.	13
Figure 1.10 Galloping Energy Harvester Designed by Sirohi and Mahadik	14
Figure 1.11 Inverted Flag Orientation Designed by Orrego et al.	16
Figure 2.1 Schematic of the Setup Giving Flag and Frame Dimensions.....	19
Figure 2.2 Construction of a Whole Model of the Harvester	20
Figure 2.3 Orientation of the Harvester in the Wind Tunnel.....	21
Figure 2.4 Wind Tunnel.....	22
Figure 2.5 Experimental Setup of High-speed Camera	23
Figure 2.6 Measurement of Flapping Parameters	24
Figure 3.1 Representation of the Flag Condition for Stable Mode in Each 8 ms in Time (AR of 1 and PR=1.1 at 2.5 m/s Wind Speed).....	27

Figure 3.2 Representation of the Flag Condition for Irregular Flapping Mode in Each 50 ms of the Time (AR of 1.5 and PR=1.1 at 5 m/s Wind Speed)	28
Figure 3.3 Representation of the Flag Condition for Regular Flapping Mode in 25 ms Time Difference in Each Image (AR of 2, PR=1.1 at 16 m/s Wind Speed).....	29
Figure 3.4 Representation of the Flag and Frame Positions in 25 ms Time for the Regular Flapping Sample (AR of 2 and PR=1.1 at 16 m/s Wind Speed)	29
Figure 3.5 Representation of the Flag Condition for Sinuous Motion Mode in 25 ms Time Difference in Each Image (AR of 1.5 and PR=1.3 at 16 m/s Wind Speed)	30
Figure 3.6 Description of Modes with Their PR and Re Numbers.....	31
Figure 3.7 Relation Between AR and PR for Each Behavior	32
Figure 3.8 Mean Flapping Frequency as a Function of Wind Speed for the Regularly Flapping Mode	34
Figure 3.9 The Effects of the Wind Speed on the Flapping Angle in the Regular Flapping Mode	36
Figure 3.10 The Relation Between St and Re Numbers in Regular Flapping Mode.....	37

ABSTRACT

Renewable energy sources are vital to reduce dependence on fossil fuels that are harmful for the environment and release greenhouse gases causing global warming. Wind energy is a natural source of energy that is abundant in the environment. While wind turbines are most popular, convenient, and used to harvest energy at large scales, there have been recent studies focusing on harvesting energy from the wind for micro devices. Such micro wind energy harvesters can decrease dependence on batteries.

In this study, a novel, framed flag micro wind harvester was designed and tested, and its behavior at three different wind speeds was experimentally examined in a wind tunnel. The main purpose of this study is to determine the geometric and wind speed conditions under which regular flapping occurs in the flag material.

A high-speed camera was used to visualize the motion of the harvester at different wind speeds and at various parametric ratios of the flag material length to the frame length. The movies taken by the camera are analyzed using Image J software to find the flapping frequency, flapping angle, and the amplitude. Nondimensional parameters such as the Re number and St number also are calculated.

This study finds that parametric ratios of 1.1 and 1.2 with the medium wind speed condition of 5 m/s are optimal flapping conditions. These optimal conditions would conveniently allow the use of piezoelectric material as the flag material in order to harvest energy. Further, an advantage of this novel design over previous designs is that the wind harvester naturally aligns with the wind direction and is thus omnidirectional.

CHAPTER 1: LITERATURE REVIEW

1.1 Renewable Energy Harvesting

Renewable energy is an environmentally friendly method to extract energy from natural sources like solar, wind, geothermal, and hydroelectric. Renewable energy has the potential to decrease our dependence on fossil fuels and thus may slow global warming by their reduction of greenhouse gas emissions and other negative environmental effects. The renewable energy sources harvested from the natural sources that are mentioned above can be either used at the macro level like solar farms and wind farms. Alternatively, renewable energy may take the form of micro-scale applications for daily energy needs and the supply of energy for microelectronic devices [1]. Types of energy harvesting are thus categorized as in Table 1.1.

Table 1.1 Types of Renewable Energy Harvesting Categorization. Adapted from Dikshit et al. 2010.

Type of Renewable Energy Harvesting	Energy Source	Solution	Ultimate Goal
Macro	Solar Wind Tidal	Energy management solutions for utility scale	Decrease fossil fuel dependency
Micro	Vibration Motion Electromagnetic Heat	Ultra-low power solutions especially for powering portable electronic devices	Driving low energy consuming devices in order to reduce dependence on batteries

Energy harvesting from wind is a productive approach to get energy from natural renewable sources for portable electronic devices. Applications of these devices, often used in outdoor applications, varies from military applications to wireless electronic devices, and unmanned air vehicles [2,3]. To supply these devices with energy, there has been a heavy dependence on battery technology, but batteries are not environmentally friendly, must be replaced periodically, and have a relatively high cost. On the other hand, extracting flow energy from either water or air, which are accessible both outdoors and indoors, is an alternative method to harvest energy in a more environmentally friendly manner [4]. Such harvesting technologies have become more prevalent with new developments in the wireless power technologies which need new and alternative power supply methods.

Several mechanisms exist to harvest energy from ambient sources like solar, wind, chemical, and thermal sources. These include piezoelectric, thermoelectric, photovoltaic, triboelectric, pyroelectric and combinations of them [5,6,7,8,9,10,11]. These main harvesting technologies are shown in Figure 1.1 [12].

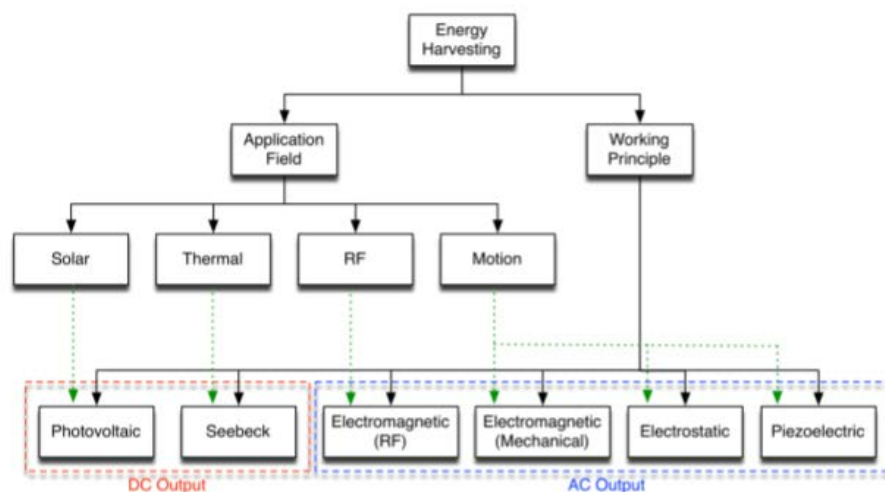


Figure 1.1 Hierarchy of Main Energy Harvesting Technologies. From "Piezoelectric energy harvesting solutions." Caliò, Renato, et al. *Sensors* 14.3 (2014): 4755-4790. CC BY-NC-SA 3.0 Reprinted with permission.

Piezoelectric materials have been utilized to harness mechanical energy by taking kinetic energy from the wind and converting it to electrical energy. This principle is a convenient way to harness wind energy in micro levels, which can be useful for devices needing small amounts of energy.

1.2 Wind Energy Harvesting

Wind energy is generally created by the difference of pressure in the atmosphere, and so air moves from a high-pressure region to a low-pressure region. This air movement is influenced by the Coriolis and centrifugal forces by the rotation of the earth, and the power occurring in the wind can be calculated with the following equation:

$$P = \frac{1}{2} \rho A u_{\infty}^3 \quad (\text{Equation 1})$$

where ρ is the density of the air, P is the power of wind, A is the cross-sectional area under consideration, and u_{∞} is the constant wind speed. From this equation, wind power changes by the cube of wind speed.

Wind energy harvesting can be categorized as macro-level harvesters or micro-level harvesters depending on their physical dimensions like length or diameter. Nabavi et al. identified 75 mm as the boundary between micro-level harvesters and macro-level harvesters [13].

Macro level wind harvesters are wind turbines which convert wind energy to rotational mechanical energy. With the technological advances materials science in terms of using cheaper, more efficient materials and different useful manufacturing methods like using composite materials in last decades, these wind turbines are now the second most used renewable energy source after solar energy. In addition, the power density of the wind is coming second most

common useful ambient source after solar energy available for outdoor energy sources shown in the Table 1.2 [13].

Table 1.2 Power Density Comparison for Ambient Energy Sources. Adapted [reprinted] from Nabavi, S., & Zhang, L. (2016). Portable wind energy harvesters for low-power applications: A survey. *Sensors*, 16(7), 1101. CC BY 4.0 Reprinted with permission.

Ambient Source	Power Density
Solar in outdoor	100 mW/cm ²
Wind at 4.47 m/s speed	10.4 mW/cm ³
Thermal at $\Delta T = 5\text{ }^{\circ}\text{C}$	60 $\mu\text{W/cm}^2$
Water drop with size of 0.35 mLat 3.43 m/s speed	30.67 $\mu\text{W/cm}^2$

1.2.1 Macro Scale Wind Energy Harvesting (Wind Turbines)

When wind (air flow) blows, low pressure air downwind pulls the turbine blades, causing them to turn by the effects of lift. Then the rotating blades turn a shaft connected to a generator, and finally, when generator rotates, electricity is produced. This principle summarizes roughly how to produce electricity by a wind turbine and is seen in Figure 1.2 [14].

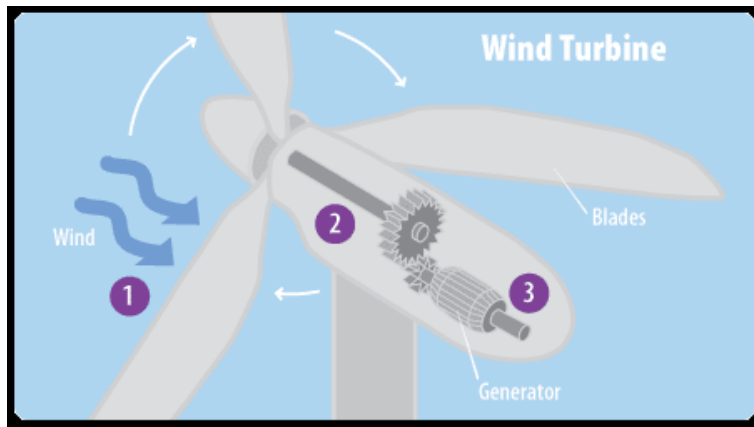


Figure 1.2 Wind Turbine Basic Operation Principle. Public Domain Image.

Wind turbines can be classified in three general ways: these are a) orientation of the axis of rotation (vertical or horizontal), b) type of aerodynamic force that rotates blades (lift or drag),

and c) energy-producing capacity (micro, small, medium, macro) [15]. The most prevalent wind turbine design is a horizontal-axis wind turbine because it has much higher efficiency than vertical-axis wind turbines [15]. Figure 1.3 includes the detailed components of a horizontal-axis wind turbine. It has generally a rotor, gearbox, a generator, and yaw system. A rotor as shown in the figure has two parts, the blades and the hub [16].

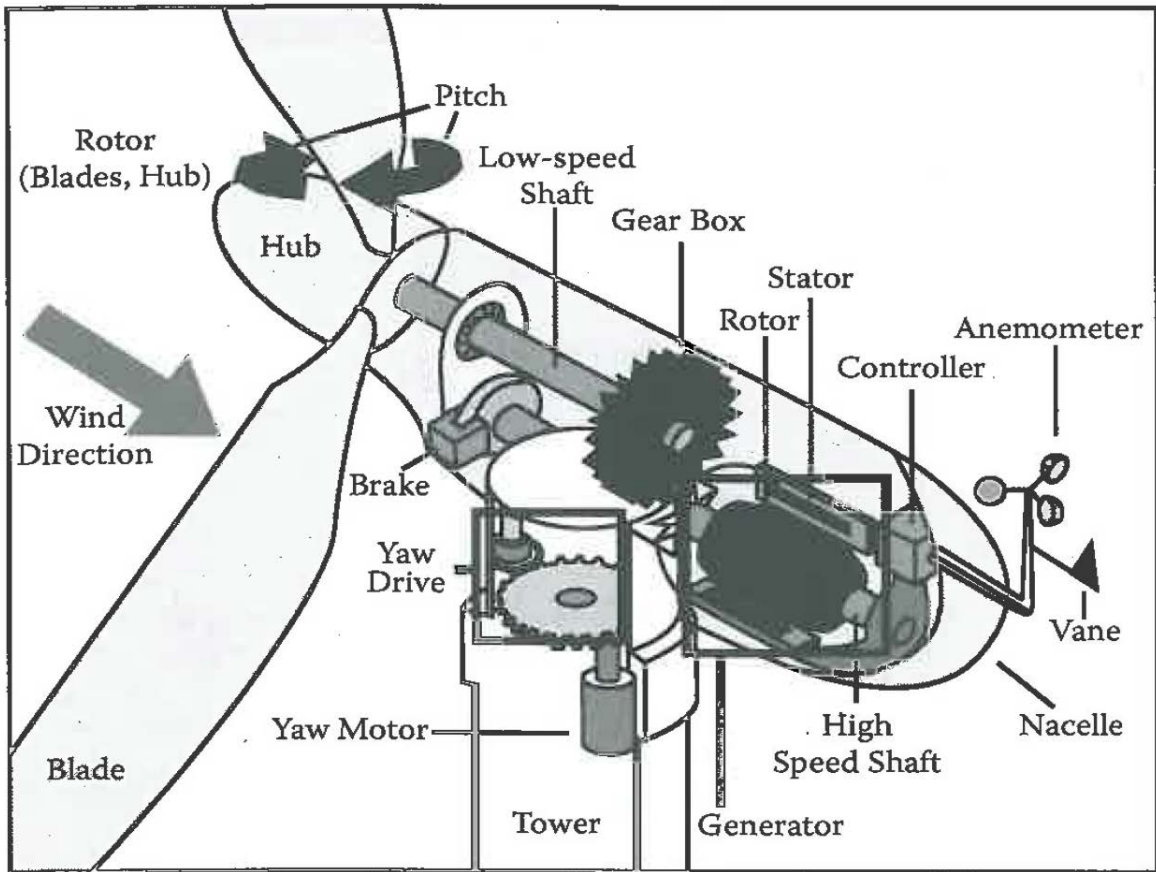


Figure 1.3 A Horizontal-Axis Wind Turbine System Components. Public Domain Image.

Another major wind turbine design is the 'Vertical Axis Wind Turbine'. In these type turbines, blades turn vertically with respect to the wind flow direction. One of the most common vertical axis wind turbines is 'Darrieus-type VAWT' that is invented by French scientist Darrieus. In this type of application, blade shapes and type can be changed by different designs to harvest more energy from wind. In addition, VAWT turbines are omnidirectional, which

means that they can scavenge wind energy from any direction thanks to the design of blades seen in the Figure 1.4 [17].



Figure 1.4 Darrieus-Type Wind Turbine. Retrieved from <https://images.nrel.gov/bp/#/folder/207425/51085242> 'NREL Image Gallery', Image number: 42794.jpg. Reprinted with permission.

1.2.2 Micro Scale Wind Energy Harvesting

Wind energy harvesting at the micro level has been explored for three decades since the wind has excellent energy potential to harness clean energy by exciting piezoelectric materials for outdoor, low power requirements. Conventionally, batteries have been used to meet the energy needs of outdoor microelectronic devices and sensors. However, since batteries have some disadvantages like replacement difficulties, high costs, and the high environmental cost of disposal, researchers have been focused on micro-scale energy harvesting technologies which may replace batteries. Tanvi Dikshit et al. [1] mentions that piezoelectric energy harvesting is a motivation to utilize clean energy because of the disadvantages of batteries stated above.

Microscale wind harvesting techniques can be categorized into two different methods, rotational harvesters and aeroelastic harvesters. In rotational harvesters, wind energy is transformed into rotational energy using the same techniques as in the large wind turbines

(explained in the previous section) but at a much smaller scale where, depending on the application, either piezoelectric materials or mechanical techniques are used to gather energy. However, for aeroelastic harvesters, the driving mechanism is to harvest wind energy by using vibration phenomena created by wind flow through the aeroelastic material properties of the harvester.

When a fluid (air in this study) flows, that flow may vibrate an aeroelastic material and aerodynamic phenomena such as vortex shedding, fluttering, and galloping may happen near or on the structure [13]. Vortex-induced vibration occurs when air flow moves around a bluff body located just before a wind energy harvester. That bluff body creates vortices that are known as ‘Karman vortices’ around the wind energy harvesters. These vortices create motion of the harvester at some frequency, and the relationship between this frequency and the Strouhal number (St) is [15];

$$St = \frac{f D}{\vec{U}} \quad (\text{Equation 2})$$

where \vec{U} is wind speed, D is the characteristic dimension (diameter for circular cylinder, hydraulic diameter for channel different than circular shapes, and chord length for wings), and f is the frequency of harvester. The Strouhal number depends not only the body shape of harvester but also Reynolds number, which is an essential dimensionless number to characterize the flow.

Re can be calculated as

$$Re = \frac{\vec{U} D}{\nu} \quad (\text{Equation 3})$$

where ν is kinematic viscosity of fluid depending on density of fluid ρ , and dynamic viscosity μ shown in the equation 4:

$$\mu = \rho \nu \quad (\text{Equation 4})$$

Common aeroelastic wind harvester mechanisms are shown in Figure 1.5 [13].

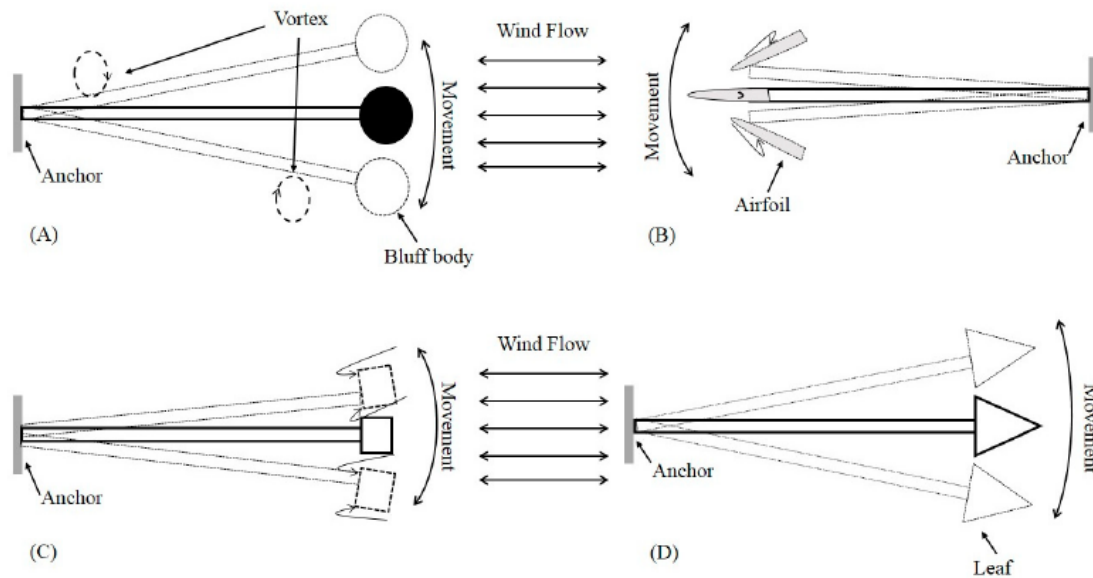


Figure 1.5 Common Aeroelastic Mechanisms for Energy Harvesting; (A) Vortex Shedding, (B) Flutter, (C) Galloping, and (D) Flapping Leaf. From Nabavi, S., & Zhang, L. (2016). Portable wind energy harvesters for low-power applications: A survey. *Sensors*, 16(7), 1101. CC BY 4.0 Reprinted with permission.

Reynolds number is one of the critical parameters to define the fluid flow and characterization of vortices that occur behind a bluff body. Flow behavior can be understood depending on Re , and it can be seen that vortices change with changing Re .

At different Re number, the effect of vortices in terms of flapping frequency and flapping angle with different amplitudes create different regimes with different vortices [18]. Flapping occurs in the fluid flow for both Re between 40 and 150 and Re higher than 3.5×10^6 [18]. Other than these two different regimes stated by Lienard, flapping cannot be seen in the desired level of vibration which triggers a flag to flap.

Vibration is a usually undesirable effect on structures like bridges, buildings, and traffic signs, but, in the application of wind energy harvesters, it can be a beneficial effect through the use of piezoelectric materials. When a mechanical load happens on the piezoelectric material,

electrical potential occurs due to the electron and proton separation inside the material by the load. This electrical potential difference can be easily converted to electrical energy with a simple circuit.

1.3 Micro Wind Harvester Designs

Micro wind harvesters can be categorized by the physical principle of how they scavenge energy from the wind. In this section, four different harvester designs in the literature are reviewed. These are i) rotational wind harvesters, ii) piezoelectric cantilever type harvesters, iii) vibration induced harvesters, iv) flag-like harvesters. These types of designs are reviewed with their conceptuality, methods, and results.

i) Rotational wind harvester designs:

In these applications, the harvester mechanism is similar to the one used in wind turbines. Wind flow rotates the blades of the turbine, and this rotational energy is converted to linear energy which excites the piezoelectric based material.

One of the best examples of the rotational harvester is called ‘windmill’, which is designed by Priya [20]. In his research, ten bimorph transducers organized around the circumference of the device are shown in Figure 1.6. In this design; similar conventional windmill design like harvester was used with the blades made up piezoelectric material. When wind reaches around the harvester, the blades of the windmill turns and by means of this rotation piezoelectric bimorph blades vibrates inside the pitch up to the stopper.

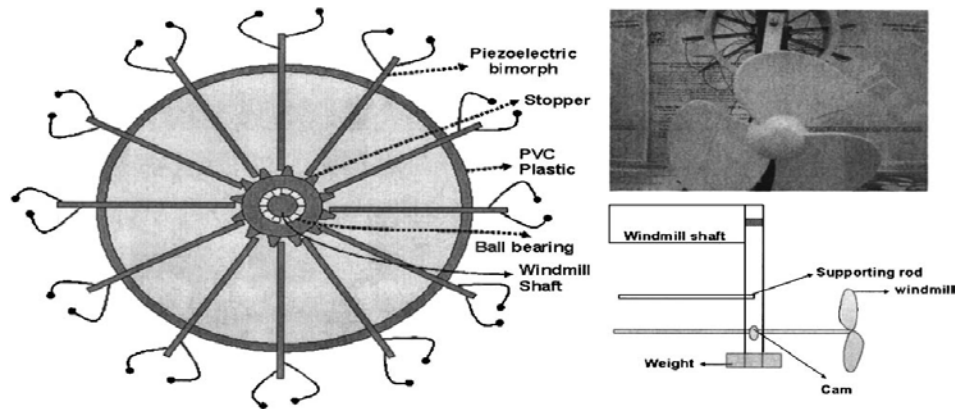


Figure 1.6 Configuration of Piezoelectric Windmill Design by Priya. From Priya, S. (2005). Modeling of electric energy harvesting using piezoelectric windmill. *Applied Physics Letters*, 87(18), 184101. Copyright © 2005 American Institute of Physics. Reprinted with permission.

Another rotational piezoelectric energy harvester created by Zhang et. al [21] using rotational piezoelectric harvester consists of turntable with three blades, PVDF (polyvinylidene fluoride) beam, rotating shaft, and fan. The operation principle of their design is converting the rotational movement to periodic oscillation on the PVDF beam. When air flow rotates the fan, turntable rotates by means of rotating shaft attached to fan and blade touches the PVDF beam. They obtained maximum output power of $2566.4\mu\text{W}$ at the wind speed of 14 m/s with their design.

In the ‘piezoelectric compact wind turbine’ design created by Karami et al. [22] They put magnets just under the disc which blades attached to, in order to create electromagnetic induction between them to tip magnets with different orientation of the magnets. In figure 1.7 the configuration of magnets with the compact turbine design is shown.

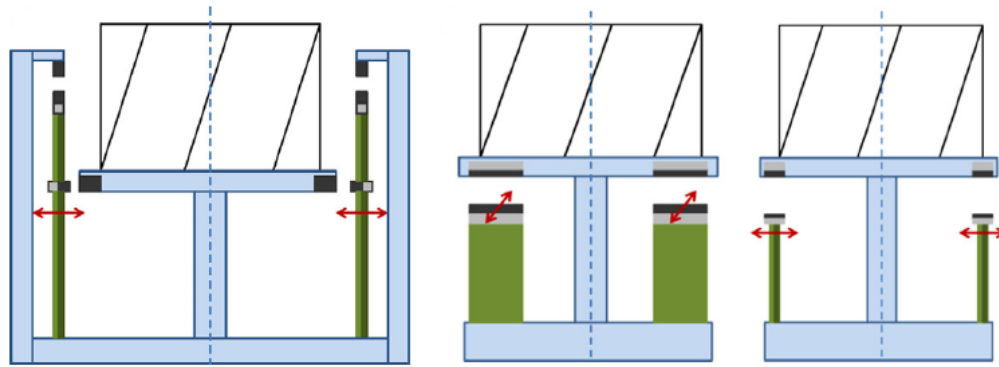


Figure 1.7 Configuration of a Piezoelectric Compact Wind Turbine. From Karami, M. A., Farmer, J. R., & Inman, D. J. (2013). Parametrically excited nonlinear piezoelectric compact wind turbine. *Renewable energy*, 50, 977-987. Copyright © 2012 Published by Elsevier Ltd. Reprinted with permission.

Tao et al.[23] proposed a piezoelectric harvester design that relies on converting rotational motion to linear motion using a “Scotch yoke” mechanism attached to the wind turbine by a shaft and attached to a piezoelectric bar by a spring. In their design, when air flow rotates the three-bladed wind turbine, the Scotch yoke mechanisms converts the rotational motion to linear motion, which induces piezoelectric bars in different sides by two different springs and levers. This device with its components and mechanisms is shown in the Figure 1.8. Their research results demonstrate that there is a possibility to reach up to power of 150 W with this harvester in designated wind speed and angular velocity conditions that are 7.2 m/s and 50 rad/s, respectively.

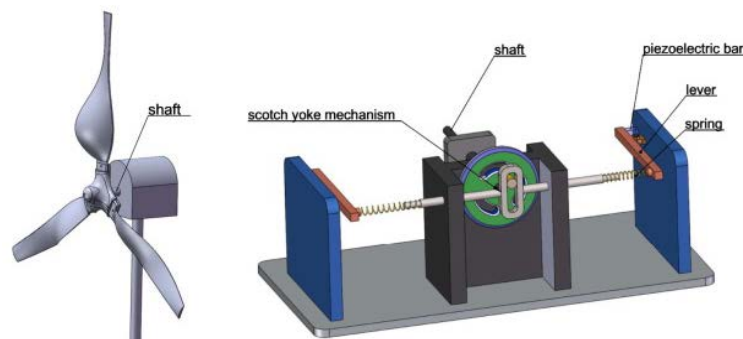


Figure 1.8 Design of Piezoelectric Wind Harvester with Scotch Yoke Mechanism. From Tao, J. X., Viet, N. V., Carpinteri, A., & Wang, Q. (2017). Energy harvesting from wind by a piezoelectric harvester. *Engineering Structures*, 133, 74-80. Copyright © 2016 Elsevier Ltd. All rights reserved. Reprinted with permission.

ii) *Piezoelectric cantilever type harvesters;*

Taylor et al. [24] came up with another idea called “eel”, which uses piezoelectric strips actuated by surface ocean waves (in the water) instead of air flow. Li and Lipson [21] used the similar technique with Taylor et al. [24] but with airflow excitation by vortex induced vibration (VIV) to harvest energy from a “piezo-leaf” where polyvinylidene fluoride (PVDF) material is attached to a cantilever stalk. Their ‘piezo leaf’ design has many advantages including low cost, light weight, scalability, robust structure, attractive bio-compatible design, and easy installation, operation, and maintenance [25].

Gao et al. [4] designed a different piezoelectric flow energy harvester that they called PFEH (Piezoelectric Fluid Energy Harvester). This design comprises a piezoelectric cantilever with a cylindrical extension. In their design, the piezoelectric cantilever is fixed into the base, but other end is attached to the cylindrical extension which leads it to vibrate at the same frequency as the PFEH. In their prototypes, they used Stainless steel and lead zirconate titanate (PZT) that is thicker and stiffer than polyvinylidene fluoride PVDF but has a higher piezoelectric coefficient to compare their behaviors. They reported that the voltage and generated power was higher in turbulent excitation than in laminar flow.

PVDF and PZT materials were preferred in most of the studies. It is understood that PVDF is more efficient than PZT because PVDF has a higher piezoelectric coefficient, as stated by Gao et al. [4]. Vatansever [26] investigated energy harvesting from wind flow and water droplet renewable sources using PVDF and PZT. He concluded that more power can be utilized from a polymer-based material (e.g. PVDF) than from a ceramic-based material (e.g. PZT). He stated that piezoelectric polymer materials such as PVDF have much more possibility to produce

energy from both rain drops and wind. In his study, for example, maximum peak voltage was produced around 61.6 V at 10 m/s wind speed with PVDF sample (LDT4-28K).

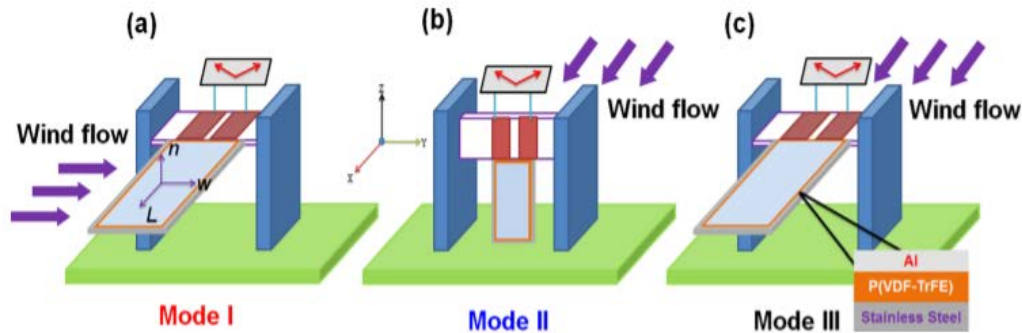


Figure 1.9 Diagram of Three Different Modes Used in the Design of Dong Jun Li et al. From Jun Li, D., Hong, S., Gu, S., Choi, Y., Nakhmanson, S., Heinonen, O., ... & No, K. (2014). Polymer piezoelectric energy harvesters for low wind speed. *Applied Physics Letters*, 104(1), 012902. Copyright © 2014 AIP Publishing LLC. Reprinted with permission.

Dong Jun Li et al. [27] fabricated a polymer piezoelectric energy harvester that is called P(VDF-TrFE) for low wind speed conditions. They tested their material in three different modes that are shown in Figure 1.9. They found that maximum power generated as $0.98\mu\text{W}$ with their new material in the Mode 1 configuration at 3.9 m/s wind velocity. This harvester designed as a cantilever beam type where piezoelectric material fixed in one side shown in the Figure 1.9 as well as with three different mode configurations in terms of the harvester configuration and wind direction.

Kwon [28] proposed a t-shaped piezoelectric cantilever to harvest energy from fluid flow. In this design, when air flow arrives from the wider side of the cantilever, it creates fluttering of the piezo ceramic elements that are patched on the base side. He stated that continuous maximum power output of 4 mW in the wind speed of 4 m/s is produced by the harvester. Another flutter-based wind energy harvester studied experimentally by Li et al. [29] used dangling crossflow fluttering instead of parallel flow fluttering. They designed and tested three different PVDF stalk that have long, short, and narrow-short stalks. In their different

experiments, these researchers measured a maximum power density of about 2 mW/ cm^3 in crossflow narrow-short stalk.

Sirohi and Mahadik [30] proposed wind energy harvesting device consisting of two piezoelectric sheets attached to the cantilever beam which creates a galloping motion due to its equilateral triangle cross section exposed to the wind flow. They compared their experimental results with an analytical model. Finally, they reported that their device produced more than 50 mW at 11.6 mph wind speed condition with the galloping phenomena shown in the Figure 1.10.

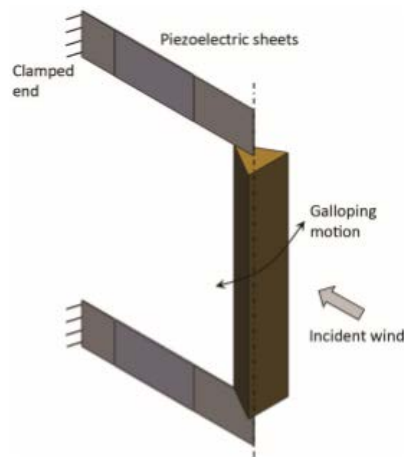


Figure 1.10 Galloping Energy Harvester Designed by Sirohi and Mahadik. From Sirohi, J., & Mahadik, R. (2011). Piezoelectric wind energy harvester for low-power sensors. *Journal of Intelligent Material Systems and Structures*, 22(18), 2215-2228. Copyright © 2011, © SAGE Publications. Reprinted with permission.

Most studies of the piezoelectric wind harvesters use designs in which the air flows in only one direction, but Zhao et.al [31] designed an arc-shaped piezoelectric harvester which provides energy from air flow coming in multiple directions. They created a new design to respond to multi-directional wind flow excitations; this design therefore has the opportunity to scavenge more energy than conventional designs. An analytical method was used to understand the behavior of an arc-shaped elastic beam as a wind harvester. Finally, in 2-17 m/s wind speed range they created 1.73 Mw maximum power output at wind speeds of 17 m/s.

iii) *Harvesters using vortex-induced vibration phenomenon;*

Weinstein et al. [32] proposed a harvester excited in heating, ventilation, and air conditioning (HVAC) flows using a vortex shedding phenomena created when vortices reach an aerodynamic fin located at the end of a piezoelectric cantilever. This study shows that piezoelectric harvesters can be used in HVAC ducts where air flow is available. They found that the power outputs generated with the proposed design were 200 μ W and 3 mW for flow speeds of 2.5 m/s and 5 m/s, respectively. They stated that these power outputs are adequate for powering wireless sensor nodes for HVAC monitoring systems or other sensors.

Sivadas and Wickenhiser [33] studied the effects of the geometry of bluff bodies using vortex-induced vibration techniques on the power output produced by piezoelectric material. Out of three different bluff body shapes (e.g. cylindrical, triangular, and pentagonal) they achieved the highest power of 0.35 Mw using the cylindrical bluff body shape at $Re=300-1100$ for a beam length of 0.04 m and diameter of 0.02 m.

iv) *Flag-like harvesters;*

Recently, Orrego et Al. [34] designed a novel inverted piezo electric flag-like wind harvester. These researchers performed experiments both in a small-scale wind tunnel but also tested their design in the field. They tested it in ambient wind conditions which have intermittency of wind and potential leakage of electrical charges into the circuit as pointed out before by Zhao L.[35] and Zhao L, Yang L.[36] respectively.

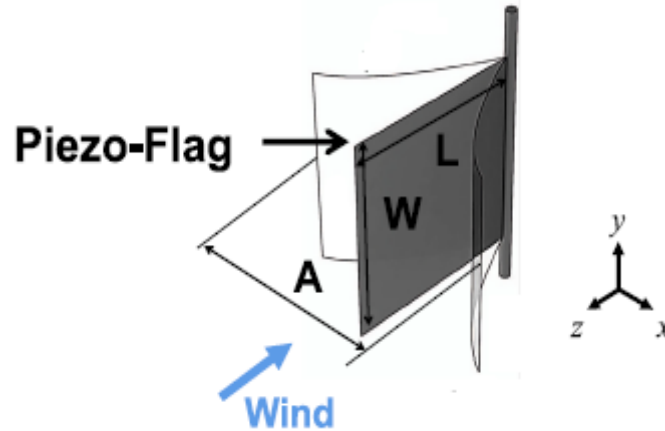


Figure 1.11 Inverted Flag Orientation Designed by Orrego et al. From Orrego, S., Shoele, K., Ruas, A., Doran, K., Caggiano, B., Mittal, R., & Kang, S. H. (2017). Harvesting ambient wind energy with an inverted piezoelectric flag. *Applied energy*, 194, 212-222. © 2017 Elsevier Ltd. Reprinted with permission.

Orrego and co workers used an inverted flag design as seen in the Figure 1.11, which means that the flag is fixed at the trailing edge (relative to the direction of the wind) and its leading edge is free to oscillate in response to air flow. These researchers tested different flag material bending stiffnesses and mass ratios to determine characteristic flapping behaviors under these conditions.

Furthermore, they tested their design in the ambient wind conditions where the wind direction could change and finally they used the harvested energy to operate a temperature sensor. As a result of their study in the wind tunnel with the controlled wind conditions, they reported that a peak electrical power of around 5.0 mW/cm^3 reached at a wind velocity of 9 m/s , while they got 0.4 mW/cm^3 even in low speed conditions around 3.5 m/s .

Silva-Leon, Jorge et. al [37] improved Orrego's and co-workers' inverted flag design by adding flexible solar panels into the inverted flag to compare and investigate their wind/solar energy harvesting device in both piezo-only design and piezo/solar design. The purpose of the solar panels was to eliminate the intermittency of power generation by the wind alone. They therefore investigated the harvesting capabilities of flexible solar panels and piezoelectric strips

attached to the inverted flags with 1.8 Klux constant light exposure in laboratory conditions at a different wind conditions available in the wind tunnel. They concluded that their total power output is around 5mW, which is the same as measured by Orrego et al.. However, they presented a novel idea with the integration of flexible solar panels that provides up to 3 mW power; these can be useful for some small-scale portable electronics when only a solar source (and no wind) is available to harvest energy.

CHAPTER 2: MODEL AND DESIGN

2.1 Introduction

In this thesis, a novel, flag-like wind harvester consisting of a flexible flag material attached at its leading and trailing edges to a surrounding rigid frame has been studied. This design fits into the flag-like wind harvester design category reviewed in Section 1.3 in terms of the physical principle used to scavenge energy from the wind. The mechanical principle in this study is the same with the flapping flag like wind harvesters. While in the inverted flag designs reviewed in Section 1.3, wind blows from the trailing (i.e. free) edge to the leading (i.e. attached) edge of an aero elastic material, in this design wind blows from the attached edge (along which the flag may pivot) to the trailing, free edge. A parametric study is conducted to determine the optimum design conditions to maximize flapping of this device.

2.2 Harvester Concept and Design

A model wind energy harvester was designed to understand the effects of air flow on a flag-like wind harvester with a rigid frame. The variables under consideration in designing this model included the ratio of the frame height to the frame length, the ratio of the frame length to the flag length, and the wind speed. Previous wind energy harvesters have used piezoelectric material to convert mechanical strain caused by the wind into electrical energy. However, before incorporating piezoelectric materials into the current model, it is essential to find optimum design conditions (which depend on the flag and frame dimensions and the wind speed) which maximize the desired reciprocating behavior. In this study, the main aim is thus to find the

optimum geometry, design, and parameters to be useful for a piezoelectric flag-like wind harvester.

2.2.1 Concept

The wind energy harvester model consists of a shaft, frame, and flag. The shaft was made of polymer-based material; it has a bearing in one end which allows the entire apparatus to rotate. Secondly, the frame was 3-D printed using PLA (Polylactic acid) filament. The flag itself was made of a flexible polypropylene plastic material chosen for its durability to wind flow. As shown in Figure 2.1, the flag material is fixed at two sides of frame using three clamps.

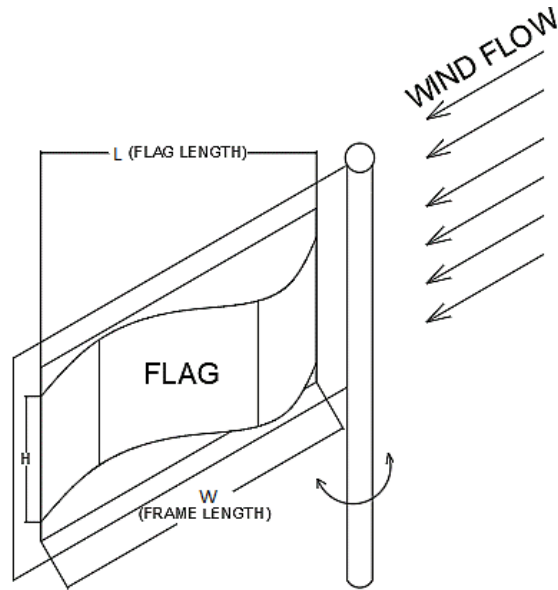


Figure 2.1 Schematic of the Setup Giving Flag and Frame Dimensions.

In this model, L stands for frame length, H stands for the flag height, and W stands for the flag length. The variable U is the wind speed. In order to determine the behavior of flags with different dimensions, a parametric ratio and the aspect ratio were used. The parametric ratio ($PR = (W/L)$) is the ratio of the flag length W to frame length L. Another ratio, the aspect ratio ($AR = (L/H)$), is the rate of the frame length L to the flag height H. Flag and frame dimensions with different parametric ratios that are 1, 1.1, 1.2, and 1.3 are shown in detail in Table 2.1. Flag

and frame dimensions were designed such that the device would fit into the wind tunnel to be described subsequently.

Table 2.1 Experimental Sample Matrix Table

FRAME DIMENSIONS (H x W) [cm]			FLAG DIMENSIONS (H x L) [cm]			
			PARAMETRIC RATIO (PR)			
			1	1.1	1.2	1.3
ASPECT RATIO (AR)	1	5x5	1) 5x5	2) 5x5.5	3) 5x6	4) 5x6.5
	1.5	5x7.5	5) 5x7.5	6) 5x8.25	7) 5x9	8) 5x9.75
	2	5x10	9) 5x10	10) 5x11	11) 5x12	12) 5x13

2.2.2 Design

The design consists mainly of three parts, the base, shaft, and harvester. In the base section, an aluminum rod, base flange, bearing flange, and bearing were used. The shaft was used to enable rotation (owing to the bearing) and to attach the harvester. The harvester in this study was designed as regular flag that is built flag material surrounded by a rigid frame. An image of the completed design is shown in Figure 2.2.

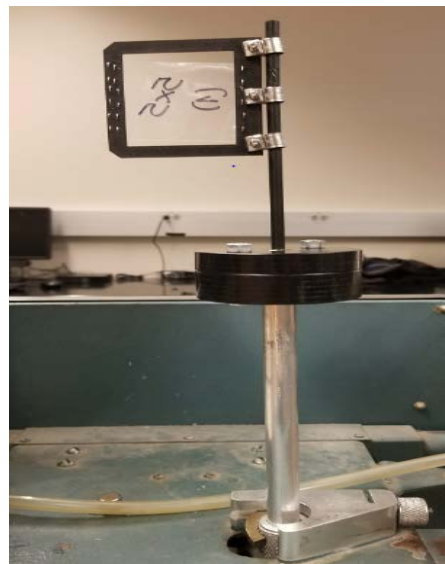


Figure 2.2 Construction of a Whole Model of the Harvester.

After the construction was done from base to the upper side of shaft, flag material is bonded to two sides of the frame with heavy duty staples. The flag with frame is attached to the shaft that is free to rotate with three clamps and the design is centered in the wind tunnel. The flag is thus free to rotate around its leading edge (where the shaft is located) and the shaft diameter (of 0.25 inches) was minimized to reduce bluff body effects on the flag, and flexible polypropylene material was used to have simultaneous motion on the flag and frame.

2.2.3 Wind Tunnel and Orientation

The harvester was oriented in the center of the wind tunnel such that the air blows from the leading to the trailing edge (i.e. as a regular flag in order to attach the harvester rod, and flanges was used below the surface of the wind tunnel. In the Figure 2.3, the orientation of the whole construction in the wind tunnel is shown.

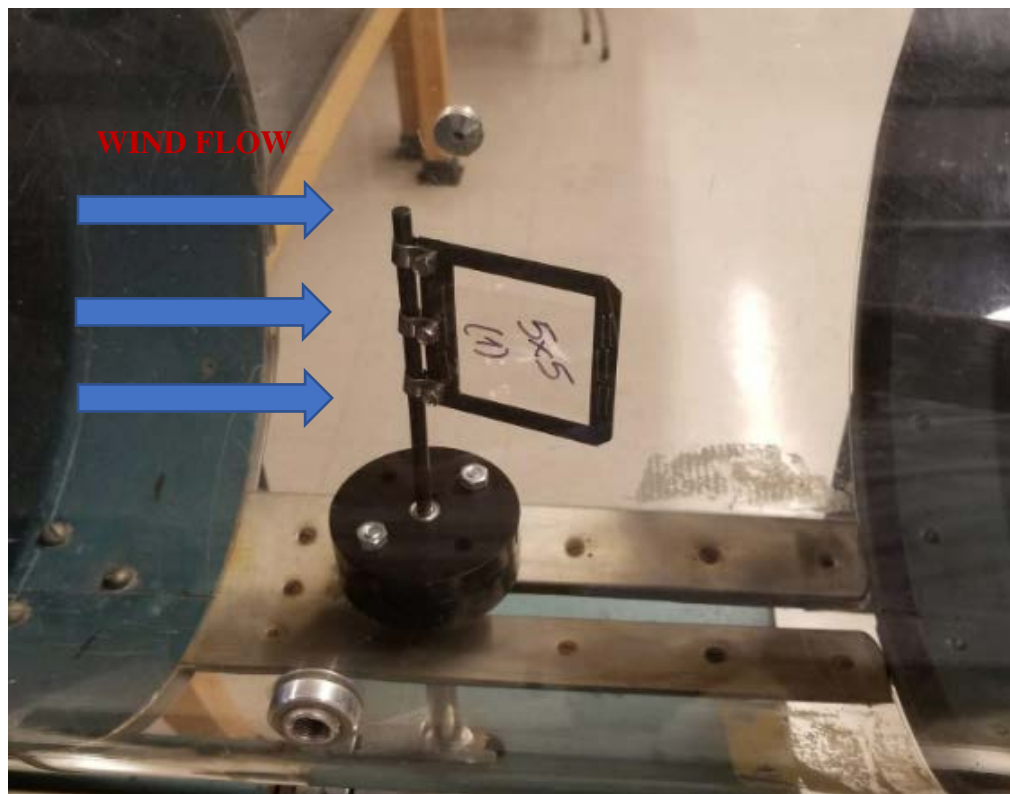


Figure 2.3 Orientation of the Harvester in the Wind Tunnel

An available wind tunnel is used to examine the behaviors of the harvester with three different wind speeds. The cross-section diameter of the wind tunnel is 12 inches.



Figure 2.4 Wind Tunnel

2.2.4 Methods

In order to systematically examine the behavior of the harvester, three parameters, the parametric ratio PR, aspect ratio AR, and wind speed U, are varied in this parametric study. PR is used to understand and find the ideal geometrical dimensions to investigate the relationship between the flag and frame lengths. Further, AR is varied to investigate how the frame height and length affect harvester performance.

Wind speed is another vital parameter in this study. Three different wind speeds were used to analyze the behavior of the harvester at different values of U. Because the speed of the fan in the wind tunnel could not be varied, the wind speed was set by increasing the resistance at the wind tunnel entrance. This was done by applying one or two layers of a fabric material at the wind tunnel entrance. While crude, this decreased wind speed from 16 m/s to 5 m/s with one layer to 2.5 m/s with two layers of fabric. These three wind speeds were measured by an anemometer (AMGAZE GM816 Digital Anemometer) in the center of the wind tunnel where the harvester was located.

Behaviors of the harvester with different parametric and aspect ratios in three wind conditions are analyzed with the videometry techniques using the high-speed camera seen in Figure 2.5. In addition to the camera two LED lights were focused on the harvester to get brighter images as well as setting the camera position thanks to the adjustable mounter. In capturing images by camera, a frame rate of 200 frames per second (fps). The camera was mounted above the test section of the wind tunnel looking downward to take videos of the flag harvester. Videos are processed in the Image J program after taken by at least 10 different measurements and the mean of the results with the standard deviation. In Figure 2.5, the orientation of high-speed camera and other tools are shown.

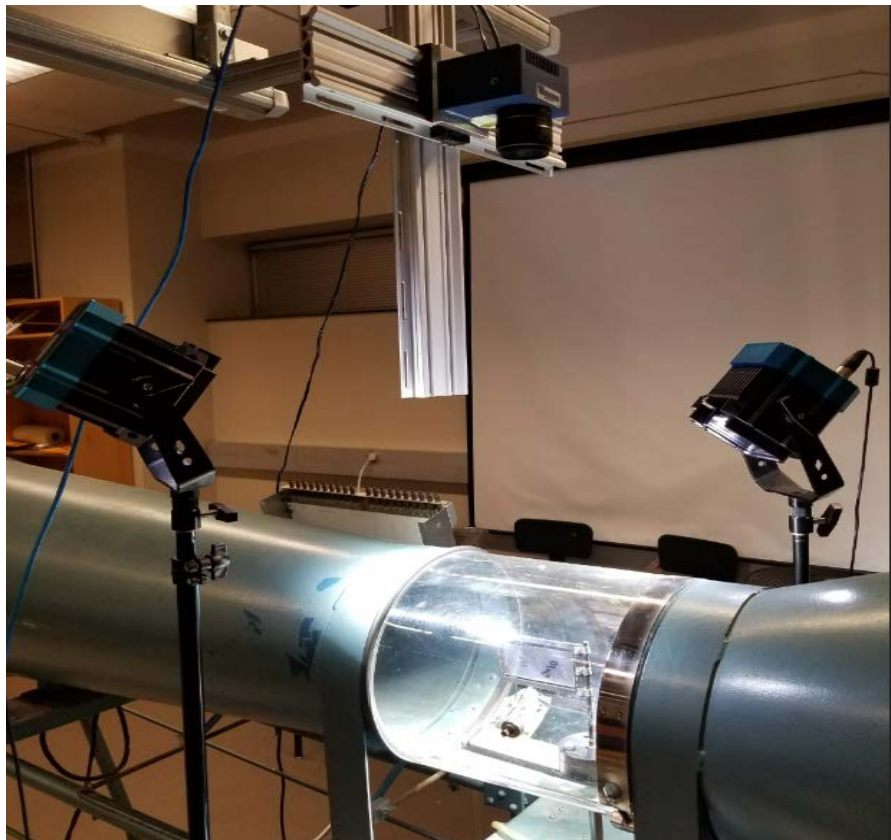


Figure 2.5 Experimental Setup of High-speed Camera

2.3 Processing and Analysis

A high-speed camera (Edgertronic SC2X-1910 fps @ 1080p) was used to see the movement of flag in three different wind speed conditions for each twelve samples to determine optimum flapping scenario. These 36-data series were analyzed in ImageJ as described below.

In ImageJ, important parameters such as flapping frequency and flapping angle were measured at minimum ten times for each sample in three different wind conditions. The mean and standard deviation of the measured values were then calculated. In addition, the flapping behavior of each set of conditions was categorized based on the video. Four different behaviors that will be discussed in detail in the next Chapter were found in this way. Flapping frequency and flapping angle were observed as a driving parameter for reciprocating mechanism in the program.

When flapping of the harvester occurs, the flapping period was defined as the time required for the flag frame to move from phase 1 to phase 2 and return to phase 1, as shown in Figure 2.6. The inverse of the flapping period then gives the flapping frequency. The flapping angle (Θ) also was measured in ImageJ using the angle measurement tool.

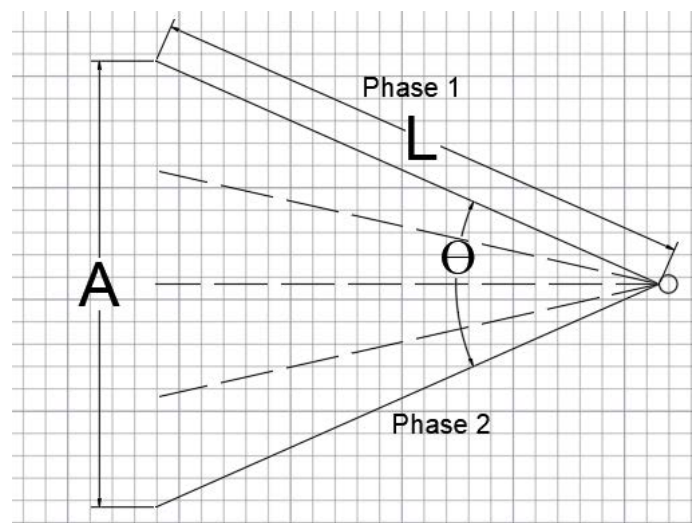


Figure 2.6 Measurement of Flapping Parameters

Flapping amplitude was calculated by the length of the frame and the flapping angle. The calculation formula using trigonometric relation is shown as in equation 4:

$$A = 2 * L * \sin\left(\frac{\theta}{2}\right) \quad (\text{Equation 4})$$

After measuring the parameters of flapping, it is essential to find the dimensionless numbers, Re and St, for defining the flapping behavior in terms of the dynamic of the wind flow. Re depends on the velocity of wind, the characteristic length (the frame length), and the dynamic viscosity of air, while St depends on flapping frequency, amplitude, and the wind velocity. These dimensionless numbers were calculated based on the following equations.

$$Re = \frac{\vec{U} L}{\nu} \quad (\text{Equation 5})$$

$$St = \frac{f A}{\vec{U}} \quad (\text{Equation 6})$$

CHAPTER 3: RESULTS

3.1 Description of Modes

Based on the recorded high-speed movies, the harvester behavior is categorized into four different flapping modes. These are a) stable b) regular flapping c) irregular flapping, d) sinuous motion. Four different modes are distributed by wind speed, the parametric ratio, and the aspect ratio. Table 3.1 shows that distribution clearly as a function of aspect ratio, parametric ratio, and wind speed. These four behaviors are described subsequently.

Table 3.1 Distribution of Harvester Behaviors in Terms of Parametric Ratio, Aspect Ratio, and Wind Speeds

FRAME DIMENSION (H x W) [cm]			FLAG DIMENSIONS (H x L) [cm] AND PROPERTIES												
			PARAMETRIC RATIO (PR)												
			1			1.1			1.2			1.3			
ASPECT RATIO (AR)	1	5x5	5 x 5			5 x 5.5			5 x 6			5 x 6.5			
			Wind velocity [m/s]			Wind velocity [m/s]			Wind velocity [m/s]			Wind velocity [m/s]			
			2.5	5	16	2.5	5	16	2.5	5	16	2.5	5	16	
		1.5	5x7.5	5 x 7.5			5 x 8.25			5 x 9			5 x 9.75		
				Wind velocity [m/s]			Wind velocity [m/s]			Wind velocity [m/s]			Wind velocity [m/s]		
	2.5			5	16	2.5	5	16	2.5	5	16	2.5	5	16	
	2		5x10	5 x 10			5 x 11			5 x 12			5 x 13		
				Wind velocity [m/s]			Wind velocity [m/s]			Wind velocity [m/s]			Wind velocity [m/s]		
		2.5		5	16	2.5	5	16	2.5	5	16	2.5	5	16	
BEHAVIOR SCALE OF FLAG EXPOSED TO THREE DIFFERENT WIND SPEED															
stable			irregular flapping			sinuous motion			regular flapping						

It is seen from Table 3.1 that regular flapping occurred for $PR=1.1-1.2$ and all values of AR . Regular flapping mostly occurred for all wind speeds at $AR=2$ but occurred for fewer wind speeds with differently shaped frames (i.e. different values of AR). Regular flapping is the preferred mode of motion because the regular flapping of the flag and oscillation of its frame facilitates extraction of energy. This mode will be analyzed further subsequently.

3.1.1 Stable

This mode describes when the flag and frame both remain stationary in response to the air flow. This lack of motion can be shown by the consecutive images taken by high speed camera in Figure 3.1, which show that the mode is defined as physically 'stable'. Images taken for the AR of the 1 with the 1.1 PR at the wind speed of 2.5 m/s are shown as a sample of this mode in the Figure 3.1 These images are separated by 8 milliseconds in time.

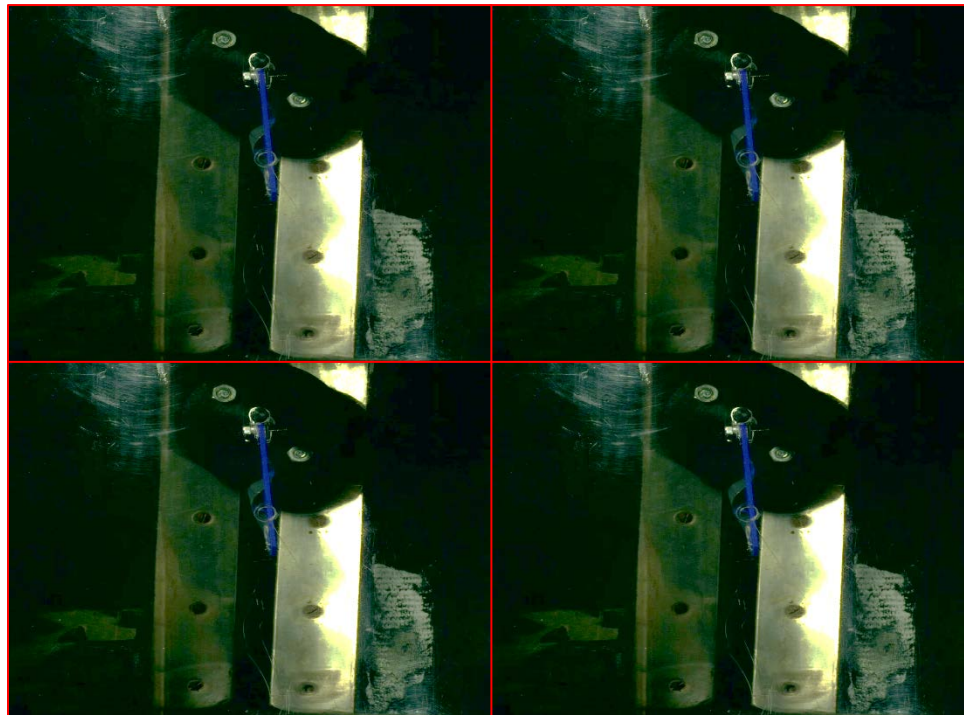


Figure 3.1 Representation of the Flag Condition for Stable Mode in Each 8 ms in Time (AR of 1 And $PR=1.1$ at 2.5 m/s Wind Speed)

In this mode, flag does not move in any direction with the different wind speed. This mode mostly occurs in the harvester when $PR=1$ and for all AR of 1 for all values of wind speed.

3.1.2 Irregular Flapping

Irregular flapping occurs when the flag flaps to some degree, but it may stop and start flapping irregularly. It is thus difficult to obtain a value of the flapping frequency and flapping angle; therefore, the flag's behavior is noted as irregular motion.

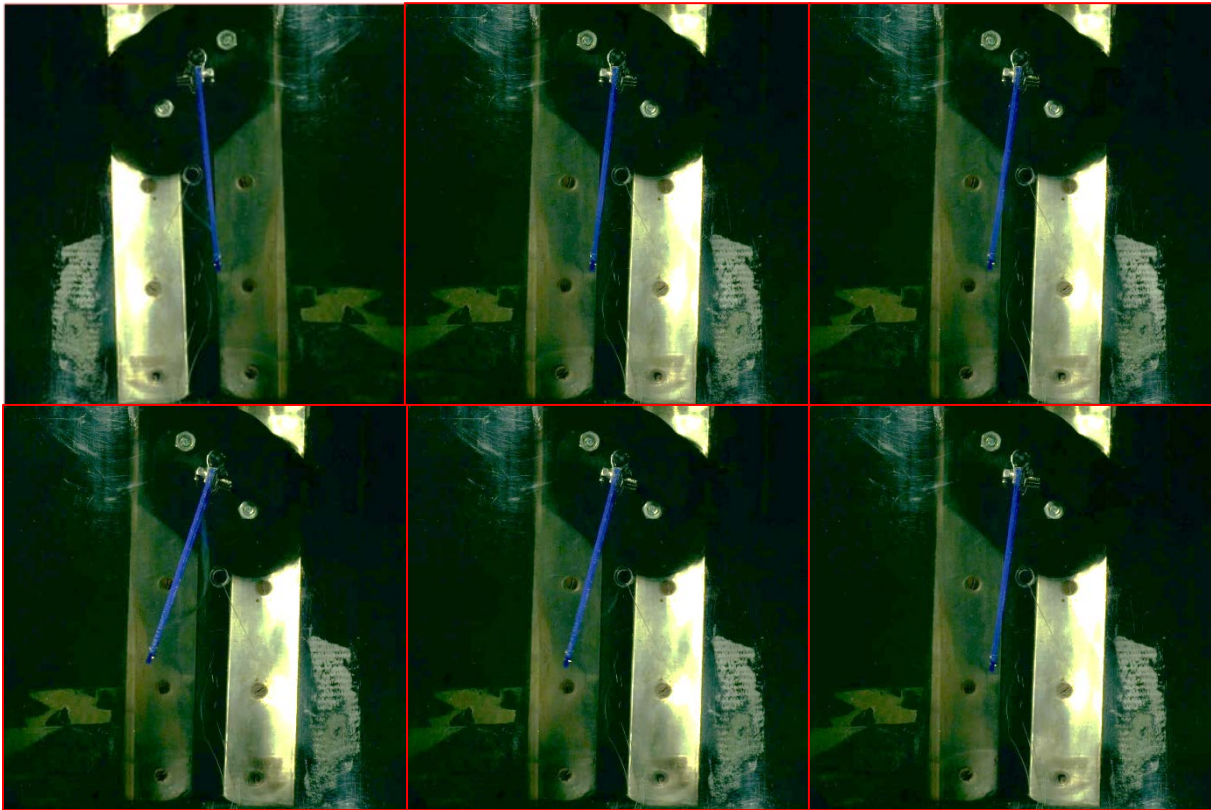


Figure 3.2 Representation of the Flag Condition for Irregular Flapping Mode in Each 50 ms of the Time (AR of 1.5 and $PR=1.1$ at 5 m/s Wind Speed)

The images for this case are separated by 50 milliseconds in time in Figure3.2. This mode as a transition between the stable mode previously described and the regular flapping mode (described subsequently).

3.1.3 Regular Flapping

Regular flapping occurs when the flag and its frame regularly oscillate from Phase 1 to Phase 2 and back again to Phase 1, as shown in Figure 3.3. In this mode, flapping frequency and the flapping angle with the amplitude can be measured exactly. It is called regular flapping because the flag material flaps as shown in Figure 3.4.

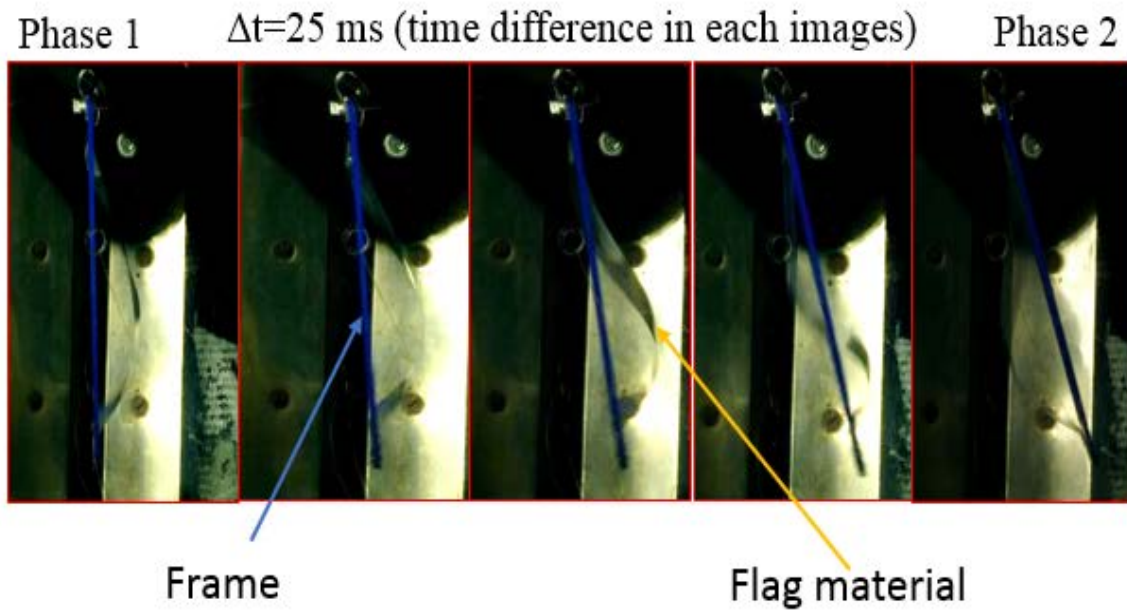


Figure 3.3 Representation of the Flag Condition for Regular Flapping Mode in 25 ms Time Difference in Each Image (AR of 2, PR=1.1 at 16 m/s Wind Speed)

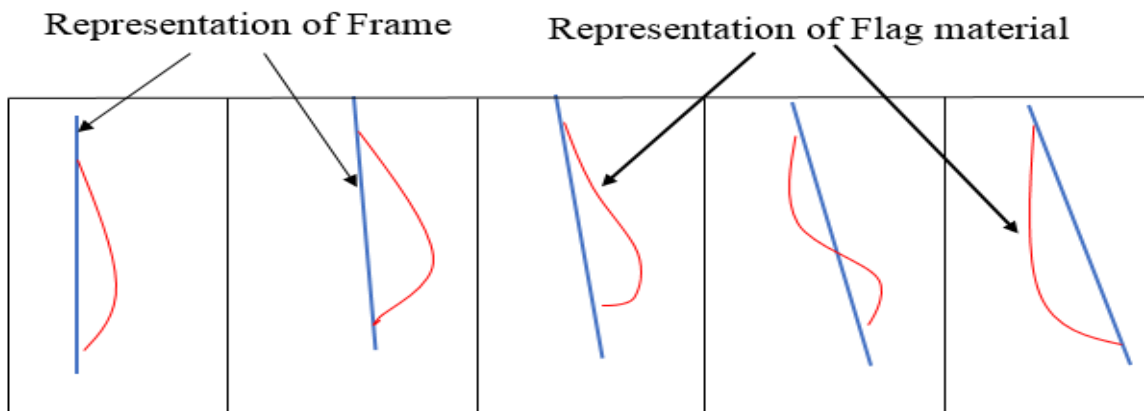


Figure 3.4 Representation of the Flag and Frame Positions in 25 ms Time for the Regular Flapping Sample (AR of 2 and PR=1.1 at 16 m/s Wind Speed)

3.1.4 Sinuous Motion

Sinuous motion occurs when the flag frame remains largely motionless, but the flexible flag material exhibits a sinusoidal, snake-like motion along the trailing edge of the flag. Because of its sinuous shape, the flag does not flap regularly with the frame. In Figure 3.5, for the sample (AR of 1.5 cm with PR=1.3 at 16 m/s wind speed) the motion of the flag is seen by consecutive images in 25 milliseconds in time.

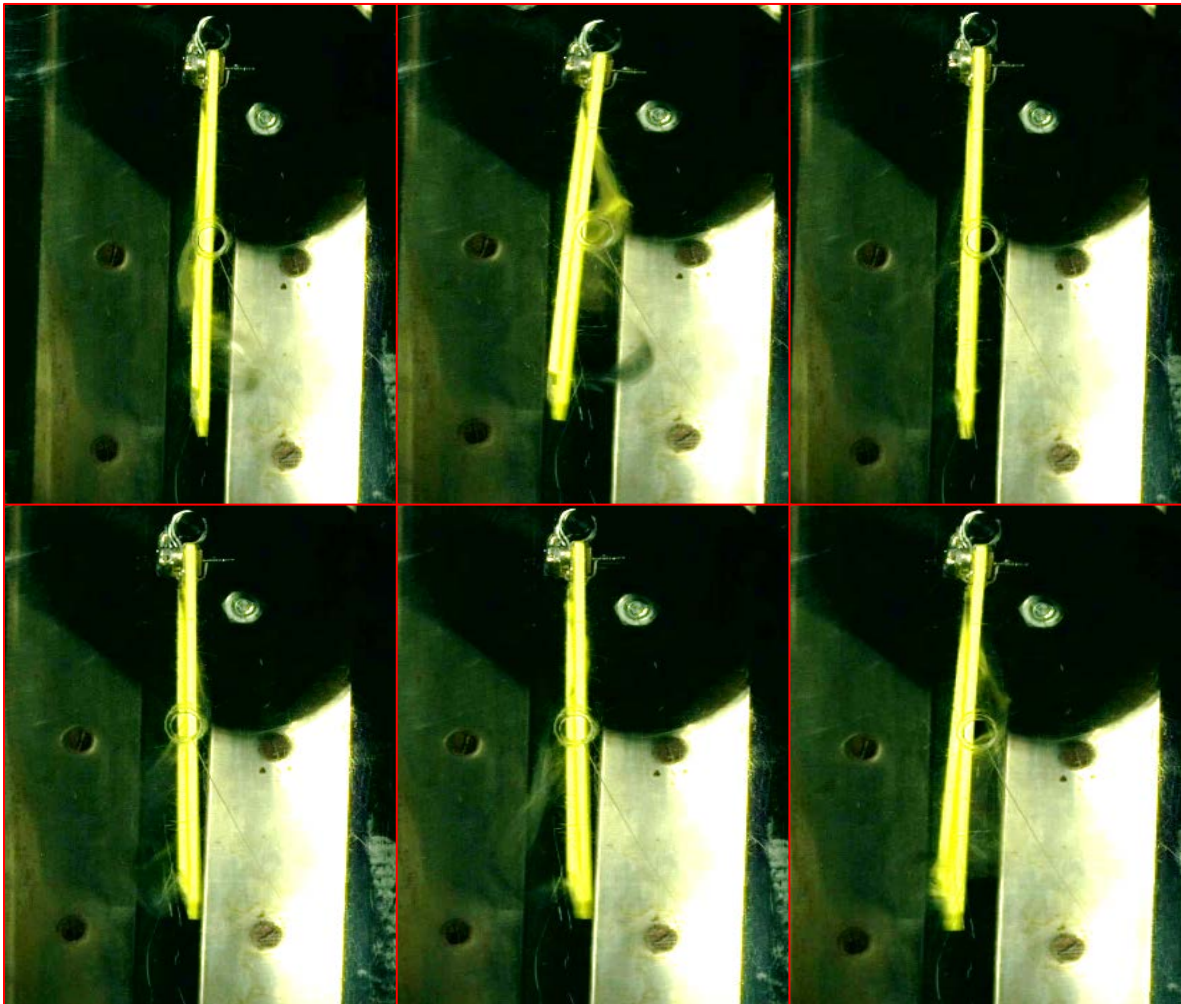


Figure 3.5 Representation of the Flag Condition for Sinuous Motion Mode in 25 ms Time Difference in Each Image (AR of 1.5 and PR=1.3 at 16 m/s Wind Speed)

This mode does not allow measurement of flapping frequency and the angle. Further, this mode mostly happens in higher wind speed and the higher parametric ratios. In higher parametric

ratios the length difference between flag material and the frame is higher than lower parametric ratios and it allows the flag material to accumulate in the trailing edge.

3.2 Analysis of The Behavior of The Flag in AR, PR, and Re

Because regular flapping is the most conducive mode to extracting usable energy, it will be the focus of the remainder of this thesis, and the other modes will not be analyzed further.

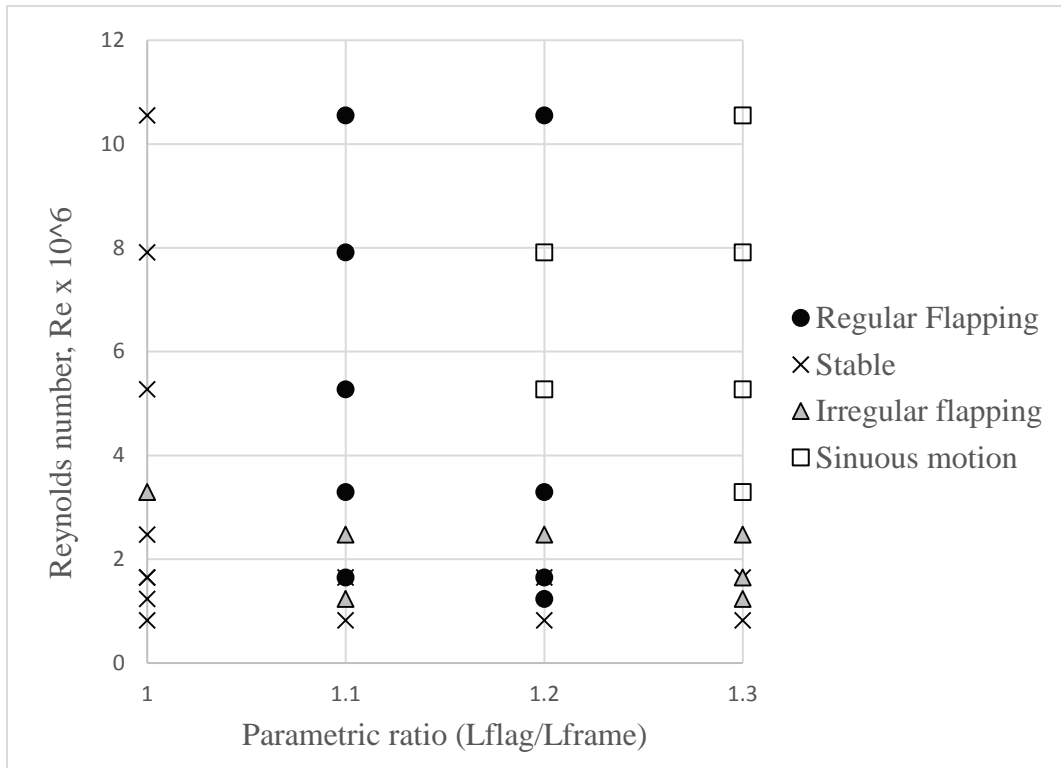


Figure 3.6 Description of Modes with Their PR and Re Numbers

Three different frame geometries were used in this experimental study. Values of the aspect ratio (AR) included 1, 1.5, and 2. The best regular flapping scenario occurred in the frames with the AR=2 because this model had more available flag material to flap and deform (and form an airfoil shape) in comparison to the two models with lower AR values.

The desired scenario of regular flapping occurred for 9 out of 36 total samples, showing that flapping occurred for one fourth of the total sample range.

The Reynolds number is another essential parameter describing the fluid dynamics. Thus, another perspective matrix was created to understand where these four modes are in terms of parametric ratio and Re number. Figure 3.6 gives this matrix in detail.

It is clearly seen that regular flapping mostly happened in the 1.1 parametric ratio flags compared to the other three modes. In Section 3.3 the behaviors and the relations between the behaviors and the parameters will be discussed in detail for regular flapping mode.

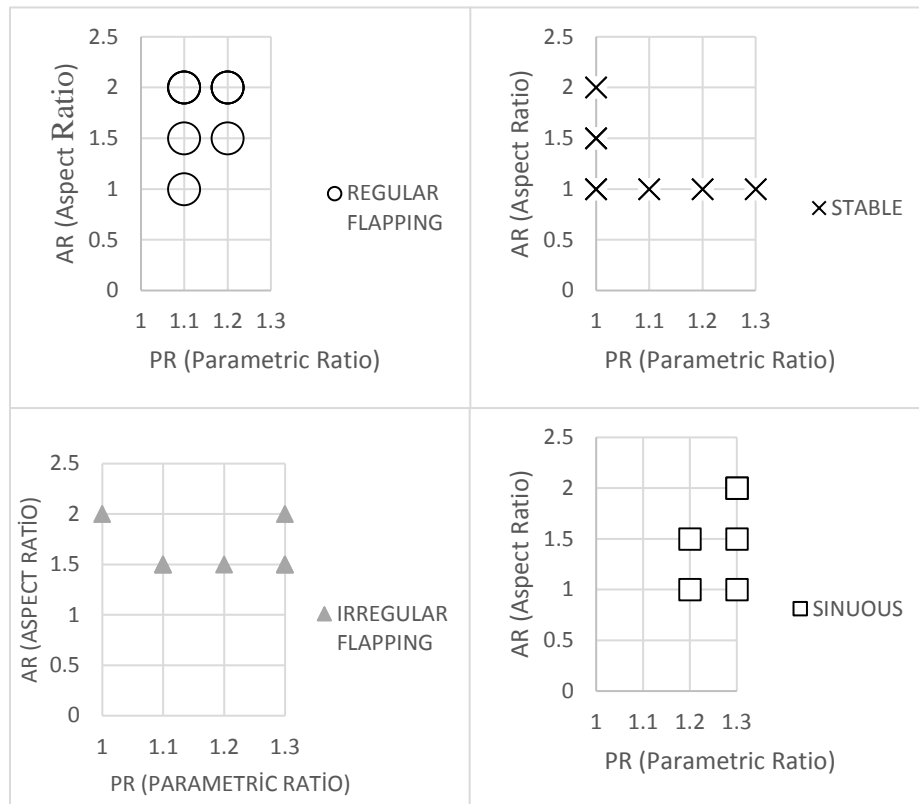


Figure 3.7 Relation Between AR and PR for Each Behavior

In this study, in terms of geometry, the optimum condition can be examined with respect to the relation between aspect ratio and parametric ratio as well as the harvester's behavior on the parametric ratio with 1.5 and 2 aspect ratios of the harvesters.

In Figure 3.7 the relationship between AR and PR for each behavior is shown. In order to understand where each behavior stands in terms of the geometric parameters that are AR and PR in this study, so the geometric features of each behavior can be seen in the figure 3.7 in detail for each mode.

3.3 Analysis of Regular Flapping

Table 3.2 shows AR, PR, wind speed, mean \pm standard deviation of flapping frequency, mean \pm standard deviation of flapping angle, and mean \pm standard deviation of flapping magnitude for experiments in which regular flapping was observed.

Table 3.2 Experimental Analyzed Values of Flapping Frequency, Flapping Angle, and the Amplitude on the Regular Flapping Samples

H (cm)	W (cm)	L (cm)	AR	PR	Wind Velocity U (m/s)	Mean Flapping Frequency (Hz)	Mean Flapping Angle (degrees)	Mean Amplitude (cm)
5	5	5.5	1	1.1	16	20.44 \pm 0.89	8.33 \pm 1.04	0.73 \pm 0.10
5	7.5	8.25	1.5	1.1	16	19.27 \pm 0.89	30.09 \pm 1.39	3.89 \pm 0.20
5	7.5	9		1.2	2.5	4.63 \pm 0.13	42.05 \pm 3.04	5.38 \pm 0.48
5	10	11	2	1.1	2.5	4.96 \pm 0.25	18.33 \pm 4.22	3.19 \pm 0.81
5	10	11			5	5.47 \pm 0.47	23.01 \pm 3.41	3.99 \pm 0.65
5	10	11			16	18.3 \pm 1.6	20.14 \pm 0.92	3.50 \pm 0.18
5	10	12	2	1.2	2.5	5.04 \pm 0.12	34.88 \pm 1.93	5.99 \pm 0.40
5	10	12			5	5.27 \pm 0.21	40.05 \pm 2.92	6.85 \pm 0.61
5	10	12			16	21.5 \pm 2.3	23.16 \pm 2.07	4.01 \pm 0.43

In this table, the mean and standard deviations of the flapping frequency for the 9 samples where regular flapping occurred are shown. It is clearly seen that the flapping frequency increases with the wind speed.

Further analysis of the regular flapping mode was performed using relationships including U (wind velocity) vs Θ (flapping angle), U vs f (flapping frequency), and Re vs St . For example, Figure 3.8 shows the flapping frequency plotted as a function of the wind speed.

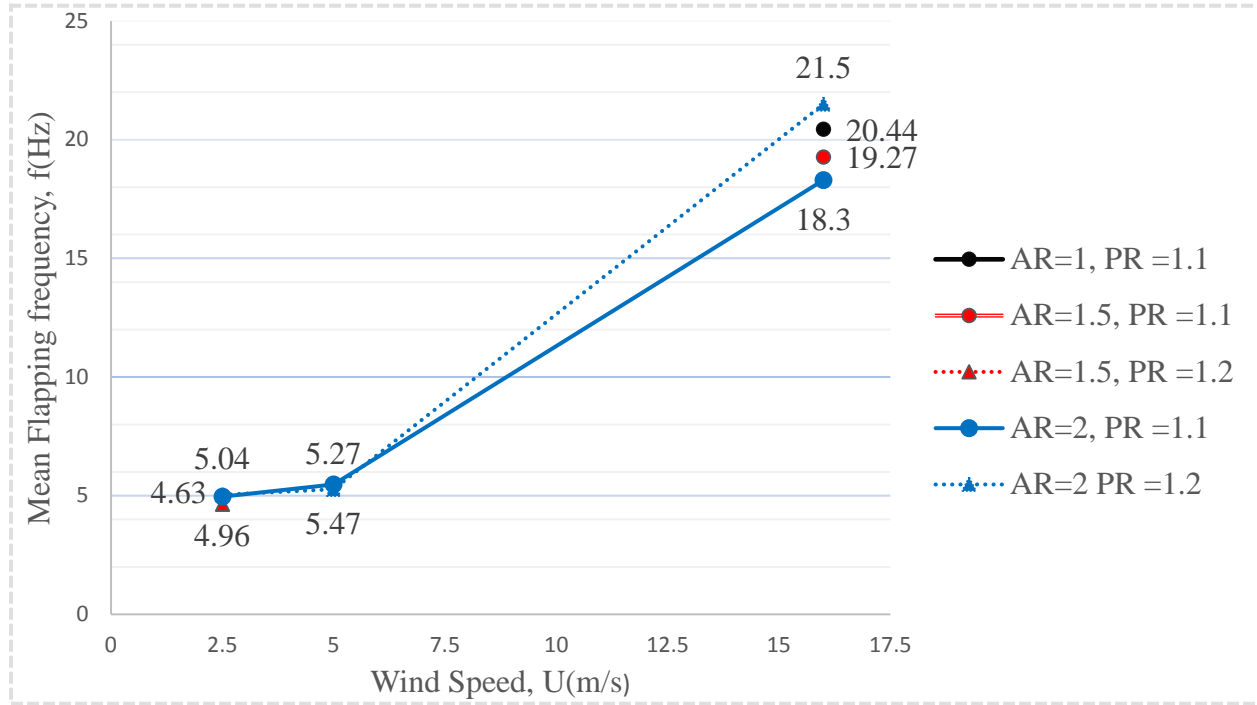


Figure 3.8 Mean Flapping Frequency as a Function of Wind Speed for the Regularly Flapping Mode

It is obviously seen that flapping frequency rises with wind speed in all cases. The lowest flapping frequencies (around 5 Hz) are seen in the lowest wind speed of 2.5 m/s, and medium frequencies (around 5.3 Hz) are noticed in the wind speed of 5 m/s while the highest flapping frequencies (about 20 Hz) are detected in the highest wind speed (of 16 m/s).

In order to understand the behavior of the wind speed with the AR and PR, the sample $AR=2$ and a parametric ratio of $AR=1.1$ or $AR=1.2$ allows further examination of flapping frequency for each wind speed condition. The flapping frequency in the wind speed of 2.5 m/s for the $AR=2$ and $PR=1.1$ is 4.96 Hz and it increases to 5.47 Hz in medium speed and to 18.3 Hz

in the high wind speed (of 16m/s). When the PR=1.2 for the same AR (of 2), the flapping frequency rises from 5.04 Hz to 5.27 and to 21.5 Hz, which is the highest possible frequency measured. In other words, for the same AR, an increase in PR from 1.1 to 1.2 also increased the flapping frequency. Regular flapping occurs for all wind speed conditions in just two different aspect ratios that are 1.5 and 2 with the two different parametric ratios that are 1.1 and 1.2 in all wind speed conditions.

In the same aspect ratio of AR=2, the flag with the parametric ratio of PR=1.2 achieved a higher flapping frequency than the one with the parametric ratio of PR=1.1 because the flag formed a better (e.g. higher lift-inducing) airfoil shape in the PR=1.2 case than in the PR=1.1 case. In the better airfoil shape, which occurs in the PR=1.2 case, the lift force also seems to be formed closer to the trailing edge (further away from the pivot point). Thus, more torque around the flag shaft is created in this sample. For the flag which has a parametric ratio of PR=1.1 the lift force is generated around the middle point of the frame, which is closer to the pivot point than in the PR=1.2 case (both for the same aspect ratio of AR=2). Therefore, the flapping frequency is slightly lower in the PR=1.1 case than in the case with PR=1.2. Similarly, in the samples with the same PR (PR=1.2) but with different values of AR (AR=1.5 and AR=1.2), a higher frequency is seen in the flag with the lower AR due to the same reason described above in terms of the shape of the flag material and the applied point of the lift force.

It can further be seen from Figure 3.8 that the flapping frequency does not vary much with AR or PR for a given wind speed, especially at the two lower wind speeds. Since the relation between wind speed and the flapping frequency is approximately the same for two different parametric ratios for the same frame dimensions, this relation is not adequate to

demonstrate the effect of parametric ratios for the optimum geometrical conditions with wind speed and especially other fluid dynamic parameters that are Re and St.

Figure 3.9 shows the mean flapping angle plotted as a function of the wind speed. It is given for each sample with their parametric ratios and aspect ratios.

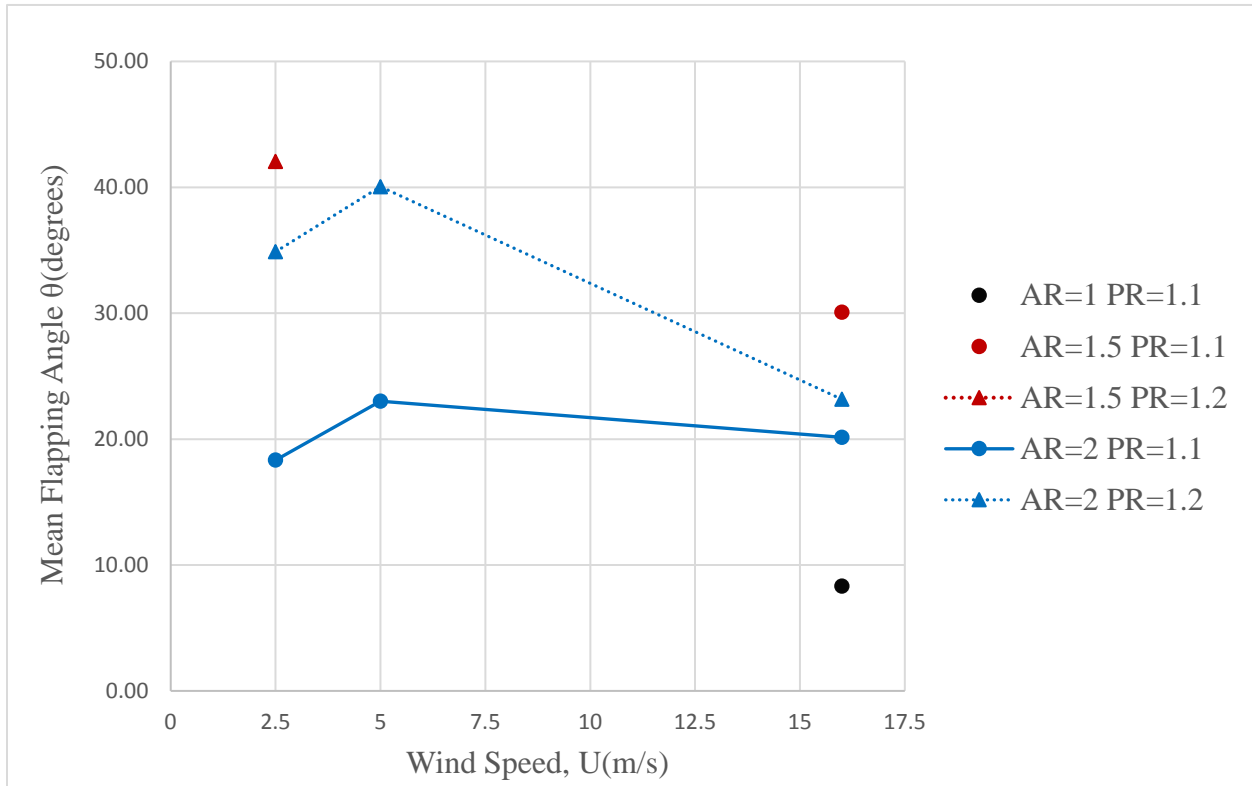


Figure 3.9 The Effects of the Wind Speed on the Flapping Angle in the Regular Flapping Mode

The same trend in flapping angle with increasing wind speed is seen for the different combinations for AR=2 and different values of PR of 1.1 and 1.2. The highest Flapping angle measured about 42 degrees for the sample with AR of 1.5 and PR of 1.2. In the samples of the same AR of 2, when the PR increases from 1.1 to 1.2 the difference is about 17 degrees in low and medium wind conditions, but in the high wind condition that is the speed of 16 m/s the difference between flapping angles for the PR of 1.1 and 1.2 is around 3 degrees.

For the comparison of the flag in the same aspect ratio of 2 with the parametric ratio of 1.1 and 1.2 flags, the flag with the PR of 1.1 has lower flapping angle than the flag with the PR of 1.2 due to the same physical reason explained for the same samples in terms of the flapping frequency.

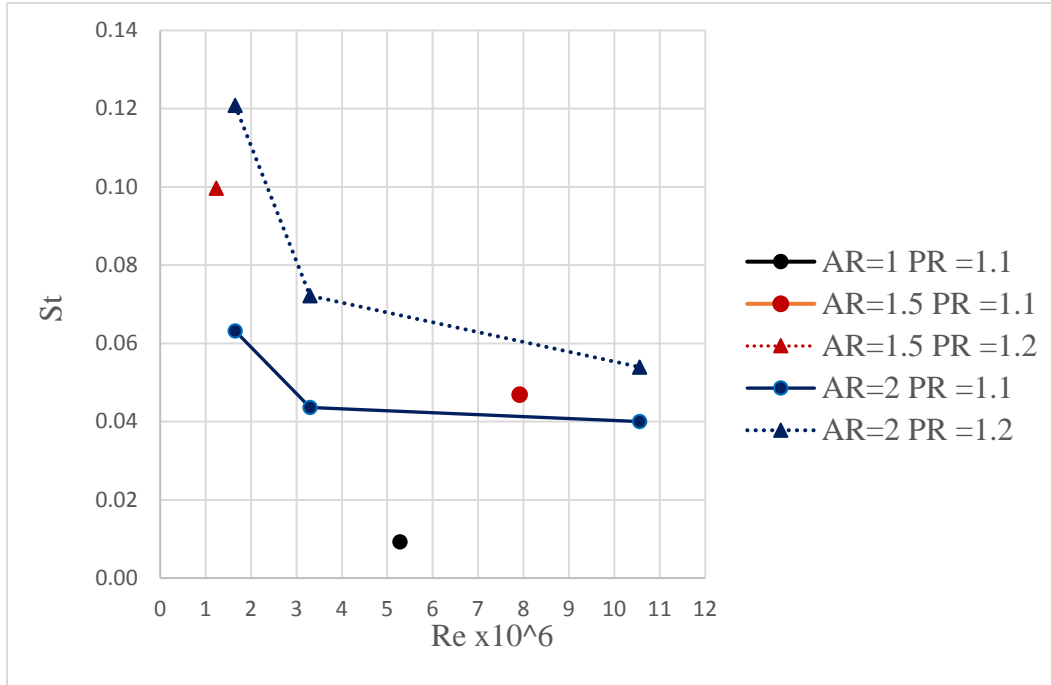


Figure 3.10 The Relation Between St and Re Numbers in Regular Flapping Mode

In the same PR of 1.1 with the AR of 1 and AR of 1.5 flag samples, the smaller flapping angle occurred with smaller values of AR (e.g AR=1) because of the flag has low inertia than the flag with AR=1.5 and so flag reciprocates in smaller flapping angles. However, the reciprocation in the case of the larger AR (AR=1.5) is larger because of the rate of the mass of the frame to the mass of the flag is greater.

In the figure 3.10, the relation between Re number and St number that are dimensionless numbers is given. It is obviously seen that in this figure, in lower Re numbers, St number is higher, and in higher Re numbers is St number is lower.

When all three of these figures are examined together, optimum features of the flag and frame begin to emerge. It seems that the 5x10 cm (AR of 2) frame with the parametric ratio of the 1.2 is ideal in lower Re number which exist in lower wind speeds. In this study maximum wind speed was 16 m/s but it is not ideal for real conditions, so optimum wind velocity is taken in this study as 5 m/s because of the other responses of parameters like flapping frequency and the St number. Further, the optimum parametric ratio would be found as PR=1.2 because the highest flapping frequency was found for this design when the aspect ratio was set to AR=2 (e.g. for the 5x10 cm frame dimensions). For further designs and improvements, piezoelectric flag material can be attached to the design instead of the plastic polymer flag material used here. This piezoelectric material should ideally be a PVDF material because it is seen in the literature that PVDF is more convenient for its flexibility and the efficiency for the wind harvesting mechanism.

CHAPTER 4: DISCUSSION

4.1 Comparison of Other Micro Wind Harvesters

This design studied here is similar to the inverted flag-like harvester studied by Orrego et al [34] in that flapping is the motion by which energy may be extracted. However, the key difference is that the harvester designed by Orrego et al. [34] is an inverted flag, where wind comes from trailing edge to leading edge while in this study the wind blows from leading edge to trailing edge.

One advantage of the current design over previous flapping designs such as that by Orrego et al [34] is that, because it can freely rotate on its shaft, it is able to gather energy from wind coming from any direction. In contrast to previous designs found in the literature which are directional harvesters, the device studied here is thus an omni-directional wind harvester design. Furthermore, the device studied here naturally aligns with the wind direction and does not have to be manually realigned, which is another advantage.

Three different wind speeds (low, medium, and high, or 2.5 m/s, 5 m/s, 16 m/s) are used in this study to examine the effects of different wind speed conditions on the harvester. However, it is understood that the high wind speed condition of 16 m/s is extremely high, is not often found in the natural world, and is not practically useful for real wind speed conditions. Therefore, the higher wind speed conditions can be neglected. The lower wind speeds studied here are more realistic and are similar to those used in previous studies.

This design is easier to design than the designs are done in the literature using a novel design that is having a frame around the flag to have an optimum reciprocation in the harvester

and optimum flapping that is vital to harvest an energy using by piezoelectric material in the flag material.

It can be understood with this study can be useful for harvesters, this study has great opportunity to have optimum responses in lower wind speed with just having 10 and 20 % longer flag material than frame length. Another advantage using this design as a harvester is, energy can be harvested by two different ways that are using piezoelectric material and rotational energy that is led by flapping angle. However rotational way is not an as attractive as piezoelectric wind harvesting option for this design because of the narrow range of the flapping angle results.

Flapping angle is important to define in terms of design conditions. For example, in this study, flapping angle was not outside of the range of the wind tunnel. In this study, flapping angle only does not show that the flapping behavior of the flag in different dynamic conditions, it must be analyzed with at least one other parameter that would be flapping frequency. Flapping angle in this study helps to detect to the amplitude, which is an important parameter to calculate Strouhal number, while the characteristic length was chosen the frame length for the calculation of the Re number.

4.2 Future Design Implementation

This novel model design was experimentally investigated as a possible method of scavenging energy from wind; however, no attempts to actually extract energy from the wind were made. In order to harvest energy, a piezoelectric material would be added to or used as the flag material instead of polypropylene plastic material currently used. This addition may possibly affect the performance of the wind harvester because the piezoelectric material would likely have a higher stiffness and mass per unit area. In addition, in the future this design should be tested in outdoor conditions to see how it behaves under ambient wind conditions.

In this study, high speed filming was used to show the flag motion in different harvester geometries and different wind conditions. To measure the harvester output power density, additional measurement devices, possibly including an oscilloscope for measuring flapping frequency and voltmeter for measuring voltage created by the piezoelectric material, would need to be added in order to compare the results with the filming results and to compare energy scavenging performance with other harvester designs

Another future application would be using two piezoelectric material strips in each side where phases are occurred to harvest energy via these piezoelectric strips when flag hits them in its flapping period from Phase 1 and Phase 2. This future implementation is also can be useful design to harvest wind energy with the integration of two piezoelectric strips to the regular framed flag.

REFERENCES

- [1] Tanvi Dikshit, Dhawal Shrivastava, Abhijeet Gorey, Ashish Gupta, Parag Parandkar, and Sumant Katiyal. Energy harvesting via piezoelectricity. *BVICAM's International Journal of Information Technology*, 2(2):265–270, 2010.
- [2] Z. L. Wang, G. Zhu, Y. Yang, S. Wang, and C. Pan, “Progress in nanogenerators for portable electronics,” *Materials today*, vol. 15, no. 12, pp. 532–543, 2012.
- [3] J. A. Paradiso and T. Starner, “Energy scavenging for mobile and wireless electronics,” *IEEE Pervasive computing*, no. 1, pp. 18–27, 2005.
- [4] X. Gao, W.-H. Shih, and W. Y. Shih, “Flow energy harvesting using piezoelectric cantilevers with cylindrical extension,” *IEEE Transactions on Industrial Electronics*, vol. 60, no. 3, pp. 1116–1118, 2013.
- [5] X. Wang, “Piezoelectric nanogenerators—harvesting ambient mechanical energy at the nanometer scale,” *Nano Energy*, vol. 1, no. 1, pp. 13–24, 2012.
- [6] G. Sebald, D. Guyomar, and A. Agbossou, “On thermoelectric and pyroelectric energy harvesting,” *Smart Materials and Structures*, vol. 18, no. 12, p. 125006, 2009.
- [7] Z. Lu, H. Zhang, C. Mao, and C. M. Li, “Silk fabric-based wearable thermoelectric generator for energy harvesting from the human body,” *Applied energy*, vol. 164, pp. 57–63, 2016.
- [8] M. Graetzel, “Solar energy conversion by dye-sensitized photovoltaic cells,” *Inorganic chemistry*, vol. 44, no. 20, pp. 6841–6851, 2005.
- [9] S. Chou, W. Yang, K. Chua, J. Li, and K. Zhang, “Development of micro power generators—a review,” *Applied Energy*, vol. 88, no. 1, pp. 1–16, 2011.
- [10] S. Wang, L. Lin, and Z. L. Wang, “Triboelectric nanogenerators as self-powered active sensors,” *Nano Energy*, vol. 11, pp. 436–462, 2015.
- [11] A. Cuadras, M. Gasulla, and V. Ferrari, “Thermal energy harvesting through pyroelectricity,” *Sensors and Actuators A: Physical*, vol. 158, no. 1, pp. 132–139, 2010.
- [12] R. Cali`o, U. Rongala, D. Camboni, M. Milazzo, C. Stefanini, G. De Petris, and C. Oddo, “Piezoelectric energy harvesting solutions,” *Sensors*, vol. 14, no. 3, pp. 4755–4790, 2014.

- [13] S. Nabavi and L. Zhang, “Portable wind energy harvesters for low-power applications: A survey,” *Sensors*, vol. 16, no. 7, p. 1101, 2016.
- [14] Retrieved from <https://www.energy.gov/eere/wind/how-do-wind-turbines-work>. ‘How do Wind Turbines Work’ by the U.S. Department of Energy. Public domain.
- [15] R.A.Kishore, C.Stewart, S.Priya. *Wind Energy Harvesting Micro to Small Scale Turbines*. Walter De Gruyter GmbH, Berlin/Boston, 2018, pp. 7-9.
- [16] Retrieved from <https://www.energy.gov/eere/office-energy-efficiency-renewable-energy> Public Domain from Office of Energy Efficiency and Renewable Energy, US Department of Energy
- [17] Reprinted from “Built-Environment Report Summary “Small Wind Conference 2016 Stevens Point, Wisconsin June 14, 2016 Slide 7.NASA Building 12, Phase 2. Photo from Mike Van Bavel.
- [18] Retrieved from <https://www.uh.edu/engines/vortexcylinders.pdf> Bulletin 300 Synopsis Of Lift, Drag, And Vortex Frequency Data For Rigid Circular Cylinders By John H. Lienhard, Figure 1 Regimes of Fluid flow around circular bluff bodies
- [19] Holmes, A. Energy Harvesting from Fluid Flows. In *Micro Energy Harvesting*; Briand, D., Yeatman, E., Roundy, S., Troccaz, J., Eds.; Wiley: Weinheim, Germany, 2015.
- [20] S. Priya, Modeling of electric energy harvesting using piezoelectric windmill, “Applied Physics Letters, vol. 87, no. 18, p. 184101, 2005.
- [21] J. Zhang, Z. Fang, C. Shu, J. Zhang, Q. Zhang, and C. Li, “A rotational piezoelectric energy harvester for efficient wind energy harvesting,” *Sensors and Actuators A: Physical*, vol. 262, pp. 123–129, 2017.
- [22] M. A. Karami, J. R. Farmer, and D. J. Inman, “Parametrically excited nonlinear piezoelectric compact wind turbine,” *Renewable energy*, vol. 50, pp. 977–987, 2013.
- [23] J. Tao, N. Viet, A. Carpinteri, and Q. Wang, “Energy harvesting from wind by a piezoelectric harvester,” *Engineering Structures*, vol. 133, pp. 74–80, 2017.
- [24] G. W. Taylor, J. R. Burns, S. Kammann, W. B. Powers, and T. R. Welsh, “The energy harvesting eel: a small subsurface ocean/river power generator,” *IEEE journal of oceanic engineering*, vol. 26, no. 4, pp. 539–547, 2001.
- [25] S. Li and H. Lipson, “Vertical-stalk flapping-leaf generator for wind energy harvesting,” in *ASME 2009 Conference on Smart Materials, Adaptive Structures and Intelligent Systems*. Citeseer, 2009, pp. 611–619.

- [26] D. Vatansever, R. Hadimani, T. Shah, and E. Siores, “An investigation of energy harvesting from renewable sources with pvd and pzt,” *Smart Materials and Structures*, vol. 20, no. 5, p. 055019, 2011.
- [27] D. Jun Li, S. Hong, S. Gu, Y. Choi, S. Nakhmanson, O. Heinonen, D. Karpeev, and K. No, “Polymer piezoelectric energy harvesters for low wind speed,” *Applied Physics Letters*, vol. 104, no. 1, p. 012902, 2014.
- [28] S.-D. Kwon, “A t-shaped piezoelectric cantilever for fluid energy harvesting,” *Applied physics letters*, vol. 97, no. 16, p. 164102, 2010.
- [29] S. Li, J. Yuan, and H. Lipson, “Ambient wind energy harvesting using cross-flow fluttering,” 2011.
- [30] J. Sirohi and R. Mahadik, “Piezoelectric wind energy harvester for lowpower sensors,” *Journal of Intelligent Material Systems and Structures*, vol. 22, no. 18, pp. 2215–2228, 2011.
- [31] J. Zhao, J. Yang, Z. Lin, N. Zhao, J. Liu, Y. Wen, and P. Li, “An arc-shaped piezoelectric generator for multi-directional wind energy harvesting,” *Sensors and Actuators A: Physical*, vol. 236, pp. 173–179, 2015.
- [32] L. A. Weinstein, M. R. Cacan, P. So, and P. Wright, “Vortex shedding induced energy harvesting from piezoelectric materials in heating, ventilation and air conditioning flows,” *Smart Materials and Structures*, vol. 21, no. 4, p. 045003, 2012.
- [33] V. Sivadas and A. M. Wickenheiser, “A study of several vortex-induced vibration techniques for piezoelectric wind energy harvesting,” in *Active and Passive Smart Structures and Integrated Systems 2011*, vol. 7977. International Society for Optics and Photonics, 2011, p. 79770F.
- [34] S. Orrego, K. Shoele, A. Ruas, K. Doran, B. Caggiano, R. Mittal, and S. H. Kang, “Harvesting ambient wind energy with an inverted piezoelectric flag,” *Applied energy*, vol. 194, pp. 212–222, 2017.
- [35] Zhao L. Small-scale wind energy harvesting using piezoelectric materials; 2015, PhD dissertation
- [36] Zhao L, Yang Y. Toward small-scale wind energy harvesting: design, enhancement, performance comparison and applicability, in press.
- [37] J. Silva-Leon, A. Cioncolini, M. R. Nabawy, A. Revell, and A. Kennaugh, “Simultaneous wind and solar energy harvesting with inverted flags,” *Applied Energy*, vol. 239, pp. 846–858, 2019.

APPENDIX A: COPYRIGHT PERMISSIONS

The permission below is for the Figure 1.1 used in Chapter 1.



[Sensors \(Basel\)](#). 2014 Mar; 14(3): 4755–4790. PMID: PMC4003967
Published online 2014 Mar 10. doi: [10.3390/s140304755](https://doi.org/10.3390/s140304755) PMID: [24618725](https://pubmed.ncbi.nlm.nih.gov/24618725/)

Piezoelectric Energy Harvesting Solutions

[Renato Calìò](#)^{1,*}, [Udaya Bhaskar Rongala](#)¹, [Domenico Camboni](#)¹, [Mario Milazzo](#)¹, [Cesare Stefanini](#)¹,
[Gianluca de Petris](#)² and [Calogero Maria Oddo](#)^{1,*}

▶ [Author information](#) ▶ [Article notes](#) ▶ [Copyright and License information](#) ▶ [Disclaimer](#)

[Copyright](#) © 2014 by the authors; licensee MDPI, Basel, Switzerland.

This article is an open access article distributed under the terms and conditions of the Creative Commons Attribution license (<http://creativecommons.org/licenses/by/3.0/>).

The permission below is for the Table 1.2 and Figure 1.5 used in Chapter 1.



[Sensors \(Basel\)](#). 2016 Jul; 16(7): 1101. PMID: PMC4970146
Published online 2016 Jul 16. doi: [10.3390/s16071101](https://doi.org/10.3390/s16071101) PMID: [27438834](https://pubmed.ncbi.nlm.nih.gov/27438834/)

Portable Wind Energy Harvesters for Low-Power Applications: A Survey

[Seyedfakhreddin Nabavi](#)^{*} and [Lihong Zhang](#)

Stefano Mariani, Academic Editor

▶ [Author information](#) ▶ [Article notes](#) ▶ [Copyright and License information](#) ▶ [Disclaimer](#)

[Copyright](#) © 2016 by the authors; licensee MDPI, Basel, Switzerland.

This article is an open access article distributed under the terms and conditions of the Creative Commons Attribution (CC-BY) license (<http://creativecommons.org/licenses/by/4.0/>).

The permission below is for the Figure 1.4 used in Chapter 1.

Hello Ahmet,

Please download the photo from our image gallery (link below). You will be required to agree to our terms and conditions, and then may use the image for your thesis.

<https://images.nrel.gov/bp/#/folder/207425/51085242>

If you run into any issues, please let me know.

Best,

Caitlin Cagle

Information Analyst | Scientific Publishing
National Renewable Energy Laboratory (NREL)
15013 Denver West Parkway, Golden, CO 80401
303.275.4192 | F 303.630.2045
caitlin.cagle@nrel.gov | www.nrel.gov

The permission below is for the Figure 1.6 used in Chapter 1.

License Details

This Agreement between University of South Florida -- Ahmet Topcuoglu ("You") and AIP Publishing ("AIP Publishing") consists of your license details and the terms and conditions provided by AIP Publishing and Copyright Clearance Center.

[Print](#) [Copy](#)

License Number	4606300320534
License date	Jun 12, 2019
Licensed Content Publisher	AIP Publishing
Licensed Content Publication	Applied Physics Letters
Licensed Content Title	Modeling of electric energy harvesting using piezoelectric windmill
Licensed Content Author	Shashank Priya
Licensed Content Date	Oct 31, 2005
Licensed Content Volume	87
Licensed Content Issue	18
Requestor Location	University of South Florida

The permission below is for the Figure 1.7 used in Chapter 1.

License Details

This Agreement between University of South Florida -- Ahmet Topcuoglu ("You") and Elsevier ("Elsevier") consists of your license details and the terms and conditions provided by Elsevier and Copyright Clearance Center.

Print
Copy

License Number	4606300588166
License date	Jun 12, 2019
Licensed Content Publisher	Elsevier
Licensed Content Publication	Renewable Energy
Licensed Content Title	Parametrically excited nonlinear piezoelectric compact wind turbine
Licensed Content Author	M. Amin Karami, Justin R. Farmer, Daniel J. Inman
Licensed Content Date	Feb 1, 2013
Licensed Content Volume	50
Licensed Content Issue	n/a
Licensed Content Pages	11
Type of Use	reuse in a thesis/dissertation
Portion	figures/tables/illustrations
Number of figures/tables/illustrations	1
Format	electronic
Are you the author of this Elsevier article?	No
Will you be translating?	No
Original figure numbers	Figure 1.
Title of your thesis/dissertation	Design and Testing of Reciprocating Wind Harvester
Expected completion date	Jun 2019
Estimated size (number of pages)	60
Requestor Location	University of South Florida

The permission below is for the Figure 1.8 used in Chapter 1.

License Details

This Agreement between University of South Florida -- Ahmet Topcuoglu ("You") and Elsevier ("Elsevier") consists of your license details and the terms and conditions provided by Elsevier and Copyright Clearance Center.

Print
Copy

License Number	4606300786766
License date	Jun 12, 2019
Licensed Content Publisher	Elsevier
Licensed Content Publication	Engineering Structures
Licensed Content Title	Energy harvesting from wind by a piezoelectric harvester
Licensed Content Author	J.X. Tao, N.V. Viet, A. Carpinteri, Q. Wang
Licensed Content Date	Feb 15, 2017
Licensed Content Volume	133
Licensed Content Issue	n/a
Licensed Content Pages	7
Type of Use	reuse in a thesis/dissertation
Portion	figures/tables/illustrations
Number of figures/tables/illustrations	1
Format	electronic
Are you the author of this Elsevier article?	No
Will you be translating?	No
Original figure numbers	Figure 1
Title of your thesis/dissertation	Design and Testing of Reciprocating Wind Harvester
Expected completion date	Jun 2019
Estimated size (number of pages)	60
Requestor Location	University of South Florida

The permission below is for the Figure 1.9 used in Chapter 1.



License Details

This Agreement between University of South Florida -- Ahmet Topcuoglu ("You") and AIP Publishing ("AIP Publishing") consists of your license details and the terms and conditions provided by AIP Publishing and Copyright Clearance Center.

[Print](#) [Copy](#)

License Number	4606300942752
License date	Jun 12, 2019
Licensed Content Publisher	AIP Publishing
Licensed Content Publication	Applied Physics Letters
Licensed Content Title	Polymer piezoelectric energy harvesters for low wind speed
Licensed Content Author	Dong Jun Li, Seungbum Hong, Shiyuan Gu, et al
Licensed Content Date	Jan 6, 2014
Licensed Content Volume	104
Licensed Content Issue	1
Requestor Location	University of South Florida


The permission below is for the Figure 1.10 used in Chapter 1.



[Home](#) [Account Info](#) [Help](#) [LIVE](#) [CHA](#)

Title: Piezoelectric wind energy harvester for low-power sensors
Author: Jayant Sirohi, Rohan Mahadik
Publication: Journal of Intelligent Material Systems and Structures
Publisher: SAGE Publications
Date: 12/01/2011
Copyright © 2011, © SAGE Publications

Logged in as:
Ahmet Topcuoglu
University of South Florida



[LOGOUT](#)

Gratis Reuse

Permission is granted at no cost for use of content in a Master's Thesis and/or Doctoral Dissertation. If you intend to distribute or sell your Master's Thesis/Doctoral Dissertation to the general public through print or website publication, please return to the previous page and select 'Republish in a Book/Journal' or 'Post on intranet/password-protected website' to complete your request.

The permission below is for the Figure 1.11 used in Chapter 1.

License Details	
This Agreement between University of South Florida -- Ahmet Topcuoglu ("You") and Elsevier ("Elsevier") consists of your license details and the terms and conditions provided by Elsevier and Copyright Clearance Center.	
Print Copy	
License Number	4606301249020
License date	Jun 12, 2019
Licensed Content Publisher	Elsevier
Licensed Content Publication	Applied Energy
Licensed Content Title	Harvesting ambient wind energy with an inverted piezoelectric flag
Licensed Content Author	Santiago Orrego, Kourosh Shoele, Andre Ruas, Kyle Doran, Brett Caggiano, Rajat Mittal, Sung Hoon Kang
Licensed Content Date	May 15, 2017
Licensed Content Volume	194
Licensed Content Issue	n/a
Licensed Content Pages	11
Type of Use	reuse in a thesis/dissertation
Portion	figures/tables/illustrations
Number of figures/tables/illustrations	1
Format	electronic
Are you the author of this Elsevier article?	No
Will you be translating?	No
Original figure numbers	Figure 1
Title of your thesis/dissertation	Design and Testing of Reciprocating Wind Harvester
Expected completion date	Jun 2019
Estimated size (number of pages)	60
Requestor Location	University of South Florida